

000 001 002 003 004 005 006 007 008 009 010 011 012 013 014 015 016 017 018 019 020 021 022 023 024 025 026 027 028 029 030 031 032 033 034 035 036 037 038 039 040 041 042 043 044 045 046 047 048 049 050 051 052 053 EPISTEMIC WRAPPING FOR UNCERTAINTY QUANTIFICATION

Anonymous authors

Paper under double-blind review

ABSTRACT

Uncertainty estimation is pivotal in machine learning, especially for classification tasks, as it improves the robustness and reliability of models. We introduce a novel ‘Epistemic Wrapping’ methodology aimed at improving uncertainty estimation in classification. Our approach uses Bayesian Neural Networks (BNNs) as a baseline and transforms their outputs into belief function posteriors, effectively capturing epistemic uncertainty and offering an efficient and general methodology for uncertainty quantification. Comprehensive experiments employing various BNN baselines and an Interval Neural Network for inference on the MNIST, Fashion-MNIST, CIFAR-10 and CIFAR-100 datasets demonstrate that our Epistemic Wrapper significantly enhances generalisation and uncertainty quantification.

1 INTRODUCTION

In the realm of machine learning, particularly in classification tasks, uncertainty estimation plays a crucial role in enhancing the robustness and reliability of models (Sale et al., 2023). Accurately quantifying uncertainty is vital for applications where decisions must be made with confidence, such as in medical diagnosis (Lambrou et al., 2010), autonomous driving (Fort & Jastrzebski, 2019) and financial forecasting. Traditional deterministic neural networks, while powerful, cannot often effectively capture and express uncertainty (Liu et al., 2020). This shortfall has spurred interest in probabilistic approaches, with Bayesian neural networks (BNNs) emerging as a promising solution in this context. BNNs offer a principled approach to uncertainty estimation by incorporating prior distributions over the model parameters, leading to posterior distributions that reflect model uncertainty (Jospin et al., 2022). Despite their theoretical appeal, BNNs face practical challenges, including high computational costs and complexity in training.

The literature majors on two sources of uncertainty: *Epistemic* Uncertainty (EU) and *Aleatoric* Uncertainty (AU) (Hüllermeier & Waegeman, 2021; Abdar et al., 2021). Epistemic uncertainty is due to a lack of knowledge about the true model parameters and can be reduced with more data or better models. In contrast, aleatoric uncertainty stems from the inherent randomness in the data generation process and cannot be reduced. Over the years, various studies (Hüllermeier & Waegeman, 2021; Abdar et al., 2021) have recognised that accurately modelling parameter uncertainty can produce a variety of credible network models, which are likely to include the true underlying network model, leading to both better EU estimation and more reliable inference. In particular, *second-order uncertainty* frameworks (including belief functions Cuzzolin (2020)) can be employed to model both EU and AU, effectively expressing ‘uncertainty about a prediction’s uncertainty’ (Hüllermeier & Waegeman, 2021; Sale et al., 2023).

BNNs, as one of the prevalent method for uncertainty estimation, treat all the weights and biases of the network as probability distributions. The prediction of the Neural Network is represented as a second-order distribution, thus representing the probability distribution of distributions (Hüllermeier & Waegeman, 2021). Although effective approximation techniques have been developed, such as variational inference (VI) approaches (Blundell et al., 2015; Gal & Ghahramani, 2016) and sampling methods (Neal et al., 2011; Hoffman et al., 2014), the high computational cost of BNNs during training as well as inference time limit their practical adoption, especially in real-time applications (Abdar et al., 2021).

Recent work shows that epistemic uncertainty (EU) can be better captured by frameworks more general than probability distributions Cuzzolin (2024), including credal sets Levi (1980) and belief

functions Shafer (1976), leading to improved robustness and uncertainty estimation Manchingal & Cuzzolin (2022); Manchingal et al. (2025b; 2023); Chan et al. (2024); Wang et al. (2024b;a); Caprio et al. (2024); Manchingal et al. (2025a).

Still, current efforts model (epistemic) uncertainty in the model’s *target* space, rather than its *parameter* space.

This paper proposes *Epistemic Wrapper*, a novel method which, for the first time, models EU in the parameter space via a random set representation by ‘wrapping’ a learnt Bayesian posterior in the form of a *belief function* (Fig. 1). The methodology unfolds organically, beginning with a Bayesian Neural Network (BNN) and culminating in an Interval Neural Network (INN). From a pre-trained BNN, we obtain posterior distributions with parameters (μ, σ) , where Gaussian priors are assumed. These posterior distributions are truncated and we compute continuous belief functions over closed intervals. Through Möbius inversion, these belief functions translate into corresponding mass values. These discrete, normalized mass values are then embedded into a continuous representation by fitting a Dirichlet distribution with parameters estimated via the method of L-moments. The interval-valued nature of Dirichlet sampling motivates the use of an Interval Neural Network (INN), which performs stable and calibrated inference. To our knowledge, no previous work has modelled EU in the parameter space via higher-order uncertainty measures. The motivation behind modelling epistemic uncertainty in the parameter space stems from the idea that parameter uncertainty is a primary source of EU. By representing uncertainty directly in the parameter space before it propagates to predictions, we capture model-level uncertainty in a more principled way. Modelling in the parameter space offers several advantages: (a) It provides a prior-agnostic mechanism to represent epistemic uncertainty, without relying solely on the model’s output distribution. (b) It enables structured and interpretable sampling through belief functions and Dirichlet distributions, supporting more stable and calibrated uncertainty estimates via interval-based inference. (c) It can be seamlessly integrated with existing BNNs offering flexibility and broader applicability.

Although Bayesian neural networks do, in theory, model epistemic uncertainty in the parameter space through the posterior, practical implementations rely on a *single* approximating distribution (e.g., a factorised Gaussian in variational inference or the implicit posterior of an ensemble). These are first-order representations and do not provide any second-order structure such as credal sets or random sets. Our approach differs precisely in this respect: the Epistemic Wrapper does not replace the BNN posterior, but *enriches* it by constructing a belief-function representation that yields a set of plausible posteriors rather than a single one. This produces a genuine second-order (random-set) model of epistemic variability in parameter space. Existing methods, including evidential deep learning and ensembles, operate on the predictive distribution or rely on a single posterior approximation, but do not introduce this higher-order parameter-space structure. The distinction is therefore not whether epistemic uncertainty originates in the parameter space it does but *how* it is represented. Our method constructs interval-based belief and plausibility bounds over parameters before prediction, offering a more expressive and robust characterisation of epistemic uncertainty. To the best of our knowledge, this is the first approach to build such a higher-order epistemic representation directly over BNN parameters, enabling principled model-level uncertainty quantification.

107

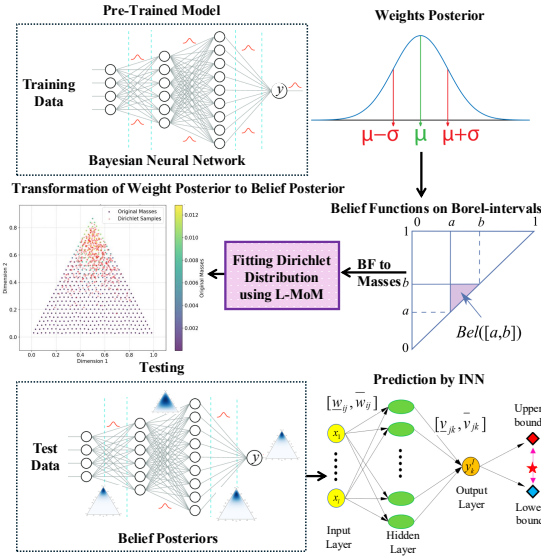


Figure 1: **Epistemic Wrapper** transforms weights posteriors from a Bayesian Neural Network into belief posteriors. It involves extracting probability posteriors, calculating belief values over Borel intervals, computing mass values using Moebius inversion, fitting a Dirichlet distribution to these masses via method of L-moments, and using the resulting belief posteriors as weights to Interval Neural Networks for final predictions.

The strength of our approach lies in the novel, careful and coherent integration of theoretically-grounded techniques. While individual components, such as belief function construction and Dirichlet fitting, are based on existing concepts, their combination into a framework that learns Random Set (RS) representations directly over BNN parameters is new and forms the core contribution of this work. In particular, the likelihood transformation at the core of our approach is not heuristic but is grounded in a set of rigorous rationality axioms. It is in fact the only belief function satisfying these properties, which provides a formal and well-founded basis for this transformation. The subsequent use of the Dirichlet mass function to encode the continuous belief function is equally principled. Our choice is guided by the need for an efficient RS representation on the collection of intervals, where any probability distribution defined over the simplex could theoretically be used. However, Dirichlet distributions have recently demonstrated strong practical effectiveness in modelling epistemic uncertainty in neural networks, as highlighted in evidential learning literature Sensoy et al. (2018). Finally, inference with INNs is also statistically motivated, as it provides an efficient way to propagate belief-based uncertainty into interval predictions. This ensures that every element of our wrapping framework is anchored in rigorous theoretical principles, rather than assembled heuristics.

Our approach leverages the strengths of BNNs while injecting the ability of higher-order measure to improve robustness and uncertainty estimation. The contributions to the literature are therefore: (1) **The first modelling of EU in the parameter space using higher-order uncertainty measures.** (2) A novel and versatile **Epistemic Wrapper** concept, that can be applied to any BNN baseline to convert it automatically into a belief-function posterior. (3) Based on the above, a **novel approach to uncertainty estimation** in classification which efficiently leverages BNNs as a foundation. Our experiments further demonstrate the versatility of the proposed Epistemic Wrapper across multiple datasets. For example, on MNIST, the baseline BNN achieved an accuracy of $72.44\% \pm 0.24$, whereas Epi-Wrapper substantially improved performance to $91.02\% \pm 0.05$. On Fashion-MNIST, the BNN reached $58.91\% \pm 0.24$, while Epi-Wrapper achieved $82.45\% \pm 0.10$. Similar improvements are consistently observed on large-scale benchmarks such as CIFAR-10 and CIFAR-100 with ResNet-18 and VGG-16 backbones, highlighting the effectiveness and scalability of our approach in enhancing predictive performance and reliability across diverse settings.

2 RELEVANT WORK

Epistemic approaches. While various types of uncertainty measures Cuzzolin (2021) have been employed in machine learning in the past Cuzzolin & Gong (2013); Cuzzolin (2018a); Liu et al. (2019); Gong & Cuzzolin (2017), recent advancements in epistemic uncertainty modelling have introduced a range of methods to improve predictive reliability across various neural architectures. Evidential deep learning predicts second-order probability distributions to estimate uncertainty, but faces challenges in optimisation and interpretation (Juergens et al., 2024). Methods like G- Δ UQ refine uncertainty calibration in Graph Neural Networks (GNNs) through stochastic data centring (Trivedi et al., 2024), while **Stochastic Partial Differential Equation (SPDE)-based GNNs** employ Q -Wiener processes for uncertainty propagation in complex graphs (Lin et al., 2024). The Graph Energy-Based Model (GEBM) leverages graph diffusion to quantify uncertainty at different structural levels (Fuchsgruber et al., 2024), and credal set-based ensemble learning constructs plausible probability distributions to measure aleatoric and epistemic uncertainty (Hofman et al., 2024).

Crucially, (Manchingal et al., 2025a) introduces a unified evaluation framework for uncertainty-aware classifiers, mapping all uncertainty-aware predictions into credal sets Cuzzolin (2008a), thus enabling a standardised assessment of epistemic uncertainty across BNNs, Deep Ensembles, Evidential Deep Learning (EDL), and Credal Set-based approaches. (Manchingal et al., 2025b) extends uncertainty modelling through Random-Set Neural Networks (RS-NNs), which employ random set theory to construct belief-based uncertainty representations, providing a more flexible alternative to conventional probabilistic models. Credal Interval Neural Networks Wang et al. (2025), instead, represent predictions as credal sets, which encapsulate a range of probable outcomes, thereby explicitly modelling epistemic uncertainty. Building on the latter, Credal Deep Ensembles (Wang et al., 2024b) predict and aggregate ensembles of convex sets of probability distributions, resulting in a more conservative and informative epistemic uncertainty quantification. In an alternative approach Charpentier et al. (2020); Malinin et al. (2019); Sensoy et al. (2018) predictions are modelled as

162 Dirichlet distributions. A key challenge with these methods is the lack of ground truth labels for
 163 uncertainty, making direct supervision difficult.
 164

165 While these models can be highly effective, they primarily quantify uncertainty at the target level,
 166 leaving the question of modelling epistemic uncertainty at parameter level open. In contrast, our
 167 proposed Epistemic Wrapper leverages BNNs to do exactly so, by transforming probability posteriors
 168 into belief posteriors, to offer a robust solution for uncertainty quantification in classification tasks.
 169

170 **Interval neural networks.** Traditional *Interval Neural Networks* (INNs) employ deterministic
 171 interval-based representations for inputs, outputs, weights, and biases, ensuring robust uncertainty
 172 modelling in neural computations. The forward propagation in an INN follows interval arithmetic
 173 principles, where the interval-formed activations in each layer are computed using element-wise
 174 interval addition, subtraction, and multiplication (Hickey et al., 2001). Specifically, the activation
 175 output of the l^{th} layer is determined by applying a monotonically increasing activation function to the
 176 interval-weighted sum of the previous layer’s outputs and the corresponding interval biases. This
 177 formulation guarantees the *set constraint* property, ensuring that for any given input and network
 178 parameters within their defined intervals, the computed activations remain bounded within a well-
 179 defined range. When the activation function is non-negative (e.g., ReLU), further simplifications allow
 180 efficient computation of interval bounds using minimum and maximum operators. This structured
 181 interval propagation enables INNs to maintain rigorous mathematical constraints while modelling
 182 uncertainties in deep learning architectures (Morales & Sheppard, 2025).
 183

184 Our approach employs INNs at inference time using our epistemic wrapper weights, sampled from the
 185 wrapped belief posterior, thus leveraging their structured interval-based representations to quantify
 186 and propagate epistemic uncertainty effectively.
 187

3 METHODOLOGY

188 **Overview:** Before presenting the full technical construction, we briefly outline the intuition behind the
 189 Epistemic Wrapper. A Bayesian neural network provides a point-valued posterior density over each
 190 weight. The wrapper enriches this by constructing a bounded random-set representation, summarising
 191 the posterior through belief and plausibility bounds. These bounds are then mapped to a Dirichlet
 192 distribution and propagated through an Interval Neural Network for inference. The following steps
 193 make this pipeline explicit. A complete step-by-step pseudo-code implementation of the Epistemic
 194 Wrapper is provided in Appendix B.1.
 195

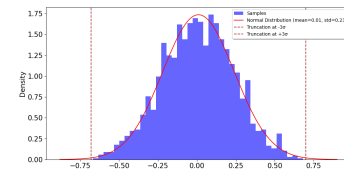
3.1 LEARNING A BAYESIAN POSTERIOR (BASELINE)

196 *Intuition.* The wrapper begins with a standard variational BNN, since it provides the posterior density
 197 we later convert into a random-set representation.
 198

199 Epistemic wrapping begins by exploiting BNNs with Gaussian priors parameterized by (μ_0, σ_0) ;
 200 training then yields posterior distributions over the weights, also parameterized by (μ, σ) . The
 201 posterior distribution $p(\omega|\mathcal{D})$ is defined via Bayes’ theorem, but is generally intractable. To address
 202 this, we employ Variational Inference, approximating $p(\omega|\mathcal{D})$ with a variational distribution $q(\omega)$ that
 203 is optimized to match the true posterior. At inference time, Bayesian Model Averaging is performed
 204 by sampling weights from the variational posterior.
 205

3.2 DYNAMIC TRUNCATION

206 *Intuition.* Since belief functions require bounded sets, we first
 207 map each posterior density to a compact interval that adapts to
 208 the scale of the learned variance. A typical Bayesian weight
 209 posterior will look like the one in Fig. 2. These posterior distributions
 210 are then truncated using a *dynamic distribution truncation*
 211 mechanism, an adaptive technique that defines the range of a
 212 distribution based on its mean and standard deviation. This
 213 dynamically scales the bounds to the parameter values according
 214 to the variance of the distribution, ensuring tighter truncation for
 215 distributions with smaller variances, where the probability mass
 216 is more concentrated, and looser bounds for those with larger
 217 variances. The truncation bounds are calculated as: Lower Bound = $\mu - \text{dynamic_multiplier} \cdot$



218 Figure 2: Posterior distribution
 219 of last-layer weights with truncation
 220 at $\pm 3\sigma$.
 221

216 σ , Upper Bound = $\mu + \text{dynamic_multiplier} \cdot \sigma$, where μ is the mean, σ is the standard deviation,
 217 and $\text{dynamic_multiplier} = \min(5.0, \frac{1.0}{\sigma})$, ensuring that the multiplier decreases for low-variance
 218 distributions while capping its value at 5.0 to prevent excessive truncation in high-variance cases. We
 219 selected this approach as it provides a balance between capturing the significant probability mass of
 220 the distribution and avoiding overly wide or narrow bounds, which could either dilute meaningful
 221 mass representation or exclude critical probabilistic regions.

223 3.3 CONTINUOUS BELIEF FUNCTIONS ON CLOSED INTERVALS

225 *Intuition.* The truncated posterior is then lifted to a belief
 226 function, providing lower and upper probability bounds that
 227 quantify epistemic imprecision in the parameter space.

228 Belief functions (Cuzzolin, 2014b) can be easily extended
 229 to continuous spaces (e.g., a network’s parameter space) by
 230 defining a continuous mass function over the collection of
 231 *closed intervals*, rather than the entire power set. For an intro-
 232 duction to belief functions, see Appendix Section A.1. Given
 233 a network parameter ω with values in \mathbb{R} , this requires defining
 234 a continuous PDF over the collection of intervals $[a, b] \subset \mathbb{R}$
 235 (Cuzzolin, 2020). Here we will assume that parameter val-
 236 ues are bounded after truncation (for illustration, in $[0, 1]$);
 237 however, the method can be easily extended to unbounded
 238 parameter values as well. The space of all closed intervals in
 239 $[0, 1]$ is a triangle, as illustrated in Fig. 3. Given a continuous
 240 mass function there (non-negative and with integral 1), one
 241 can compute the belief and plausibility value of a parameter interval $A = [a, b]$ by integrating it over
 242 specific regions of the triangle Smets (2005) (Fig. 3). The same applies for parameters bounded by
 243 arbitrary values.

244 Given a truncated posterior distribution over a network’s weights, learned by a BNN, our Wrapper
 245 transforms it into a continuous belief function using the method proposed in Wasserman (1990).
 246 For any closed interval $A = [a, b]$ of the parameter space, one can compute its *plausibility* from the
 247 posterior distribution by taking the supremum of the normalised posterior $\hat{p}(\omega|\mathbb{D})$ across all $\omega \in A$,
 namely:

$$Pl_{\Theta}(A|\mathbb{D}) = \sup_{\omega \in A} \hat{p}(\omega|\mathbb{D}). \quad (1)$$

248 The corresponding belief value is then calculated as the complement of the plausibility:
 249

$$Bel_{\Theta}(A|\mathbb{D}) = 1 - Pl_{\Theta}(A^c|\mathbb{D}), \quad (2)$$

253 ultimately providing the sought random-set representation in the parameter space.
 254

255 The method is grounded into rationality principles, such as (i) the likelihood principle, (ii) compatibility
 256 with Bayesian inference (which ensures that combining a Bayesian prior with the belief function
 257 yields the Bayesian posterior), and (iii) the principle of Minimum Commitment, which maintains that
 258 among the belief functions satisfying the previous two principles, the one chosen should commit to
 259 the least amount of information necessary Cuzzolin (2020).

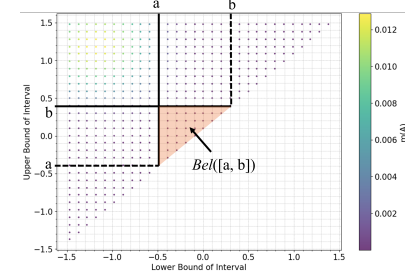
260 To cap complexity, sample belief values can be computed for a grid of parameter values only. The
 261 corresponding mass values can then be easily obtained by Moebius inversion (Shafer, 1976).

262 3.4 FITTING A DIRICHLET DISTRIBUTION

264 *Intuition.* Because the Moebius mass values lie on a probability simplex, we model them with a
 265 Dirichlet distribution, using L-moments for stable parameter estimation.

266 Epistemic Wrapper employs the method of *L-moments* Hosking (2018) to fit a Dirichlet distribution
 267 to the grid of mass values so obtained.

268 A **Dirichlet distribution** is a family of continuous multivariate probability distributions parameterised
 269 by a vector α of positive real numbers; in fact, a multivariate extension of the Beta distribution



250 Figure 3: Graphical visualisation of the continuous PDF/mass function
 251 over intervals, with the area representing $Bel([a, b])$.
 252

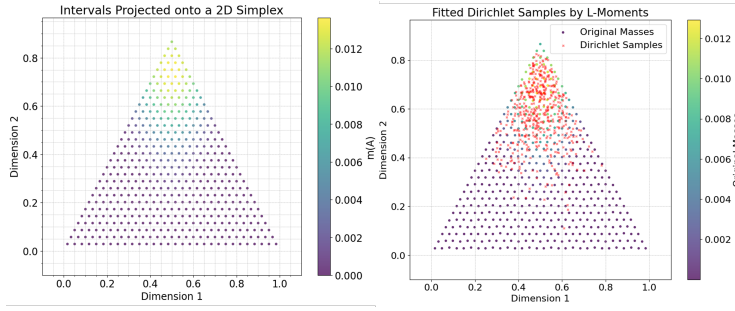


Figure 4: **Left:** Intervals projected onto a 2D simplex. Each point represents an interval $A = [a, b]$ with its location determined by the values a and b , and the colour scale indicates the corresponding mass values $m(A)$, ranging from 0.00 to 0.012. **Right:** Visualization of Dirichlet samples on a 2D simplex. Points sampled from the fitted Dirichlet distribution over mass values.

$$f(x_1, \dots, x_K; \alpha_1, \dots, \alpha_K) = \frac{1}{B(\alpha)} \prod_{i=1}^K x_i^{\alpha_i - 1}. \quad (3)$$

As they are defined on the collection of vectors $x \in [0, 1]^K$ of dimension K whose coordinates add to 1, Dirichlet distributions can be interpreted as second-order distributions. For an introduction to Dirichlet distribution, see Appendix Section A.2.

The **method of L-Moments** is a statistical approach employed for parameter estimation in probability distributions. Here we utilise this method to estimate the parameters of a Dirichlet distribution over mass values. L-moments are analogous to conventional moments but are based on linear combinations of order statistics.

To fit a Dirichlet distribution to the grid of mass values, we compute weighted L-moments from the data represented in a 3D simplex space, where each data point has an associated weight derived from its mass value. An example grid in a 2D simplex representation is shown in Fig. 4.

Computation of weighted L-Moments. We first need to compute the first-order and second-order weighted L-moments from the grid of data points. Let $\mathbf{x}_i \in \mathbb{R}^3$ denote the i -th data point in the 3D simplex and w_i its associated weight (derived by normalizing the mass values, so that $\sum_i w_i = 1$). The L-moments are computed as follows. *First-order L-moment (L_1)*. The weighted mean of the points in the simplex and is given by:

$$L_1 = \sum_{i=1}^n w_i \mathbf{x}_i. \quad (4)$$

Second-order L-moment (L_2). The weighted spread (variance) of the points relative to L_1 :

$$L_2 = \frac{\sum_{i=1}^n w_i (\mathbf{x}_i - L_1)^2}{\sum_{i=1}^n w_i} \quad (5)$$

To ensure numerical stability, a small value ϵ is added to L_2 when necessary, preventing division by zero in subsequent computations.

Using the computed L-moments, we can estimate the parameters $\alpha = (\alpha_1, \alpha_2, \alpha_3)$ of the Dirichlet distribution. The relationship between L-moments and the Dirichlet parameters is expressed as:

$$\alpha_k = L_{1,k} \left(\frac{L_{1,k}(1 - L_{1,k})}{L_{2,k}} - 1 \right), \quad k = 1, 2, 3 \quad (6)$$

where $L_{1,k}$ and $L_{2,k}$ are the respective components of the first and second L-moments along each axis of the simplex. Note that $k = 3$ corresponds to the dimensionality of the projected probability simplex. Although equation 6 can, in principle, yield negative α_k values if the second L-moment $L_{2,k}$ exceeds $L_{1,k}(1 - L_{1,k})$ (which may occur in sparse or highly skewed data), our implementation prevents this in practice. We clamp unstable L_2 values, enforce a small positive threshold ϵ on all

324 α_k . These safeguards ensure that the estimated Dirichlet parameters remain valid, positive, and
 325 numerically stable across datasets.

326 Visual representation show that, after fitting a Dirichlet distribution to the grid of mass values, samples
 327 of it are also concentrated on the top of the simplex as shown in Fig. 4-Right.

329 **Theoretical Properties of the Epistemic Wrapper.** The Epistemic Wrapper preserves an important
 330 theoretical property. Specifically, the original Bayesian posterior P lies within the credal set induced
 331 by the belief and plausibility functions after wrapping, satisfying

$$332 \quad \text{Bel}(A) \leq P(A) \leq \text{Pl}(A) \quad \text{for all measurable sets } A. \\ 333$$

334 This relation ensures that our transformation is conservative: it enriches the original posterior with
 335 second-order uncertainty without distorting the underlying predictive information. Consequently, the
 336 model maintains consistency with the Bayesian posterior while gaining robustness, which helps to
 337 explain the observed improvements in generalization and uncertainty estimation. The plausibility
 338 $\text{Pl}(A)$ captures the maximum value of $\hat{p}(\omega|\mathbb{D})$ over A , while belief $\text{Bel}(A)$ captures the minimum
 339 guaranteed mass by considering the complement A^c . Since $P(A)$ is the integral of $\hat{p}(\omega|\mathbb{D})$ over A , it
 340 must lie between the least conservative estimate (Bel) and the most generous estimate (Pl) over A .
 341 This follows from the construction rules of likelihood-based belief functions and random set theory
 342 (see Shafer, 1976; Wasserman, 1990; Cuzzolin, 2020)).

343 3.5 INFERENCE VIA INTERVAL NEURAL NETWORKS

345 *Intuition.* Dirichlet samples define weight intervals, which align naturally with the interval arithmetic
 346 of an INN and allow us to propagate epistemic uncertainty through the network.

347 Since Dirichlet sampling yields interval-based representations, the framework integrates naturally with
 348 an Interval Neural Network (for details see Appendix A.3), where weight intervals are derived from a
 349 combination of Dirichlet-based intervals (wrapped parameters) and Gaussian posteriors (unwrapped
 350 parameters). While the overall architecture follows a standard INN, our formulation integrates both
 351 Dirichlet- and Gaussian-based uncertainty representations within a unified framework. This hybrid
 352 design enables stable and well-calibrated uncertainty estimates, particularly for epistemic uncertainty,
 353 and ensures smooth interaction between wrapped and unwrapped weights during inference.

354 The unwrapped weights produced by Gaussian posteriors generate the standard bounds

$$355 \quad \underline{\omega} = \mu - \sigma, \quad \bar{\omega} = \mu + \sigma. \\ 356$$

357 In contrast, wrapped weights obtained from the Epistemic Wrapper use interval bounds induced by
 358 Dirichlet samples (see Appendix A.4). Together, these two forms of interval weights constitute the
 359 INN’s initialisation at inference time (Kim, 1993). The baseline INN uses only Gaussian-derived
 360 intervals, while the Epi-Wrapper replaces them with wrapped and unwrapped weights. Both models
 361 are subsequently fine-tuned under identical optimisation settings.

362 4 EXPERIMENTS

363 In this section, we evaluate the effectiveness of our Epistemic Wrapper in terms of uncertainty esti-
 364 mation and predictive performance. We summarize the experimental setup, including datasets, model
 365 architectures, and ablation studies, and compare our method against relevant baselines. We employed
 366 Bayesian baselines including BNNR (Auto-Encoding Variational Bayes (Kingma & Welling, 2013)
 367 with the local re-parameterization trick (Molchanov et al., 2017)), and BNNF (Flipout gradient esti-
 368 mator with the negative evidence lower bound loss (Wen et al., 2018)). We use four standard image
 369 classification benchmarks: MNIST (LeCun, 1998), Fashion-MNIST (Xiao et al., 2017), CIFAR-10,
 370 and CIFAR-100 (Krizhevsky, 2009b). Further implementation details of the Epi-Wrapper algorithm
 371 are provided in Appendix B.

372 4.1 BUDGETING

373 A budgeting strategy is introduced to selectively transform the posterior distributions of a *subset*
 374 of parameters (weights and biases). Posteriors not selected, referred to as *unwrapped* posteriors,
 375 retain their original learned parameters. We propose four distinct budgeting strategies: three are
 376 parameter-based, prioritizing posteriors with high μ , high σ , or simultaneously high μ and σ , while
 377 the fourth employs a random selection strategy that remains unbiased w.r.t. these parameter values.

378
 379 Table 1: Classification accuracies on MNIST under different budgeting criteria before and after
 380 fine-tuning for posterior weights. Results are from 15 runs. Best scores are presented in bold.

381 BUDGETING	382 MLP SIZE	383 BEFORE FINE-TUNING		384 AFTER FINE-TUNING		
		385 INN	386 EPI-WRAPPER	387 BNN	388 INN	389 EPI-WRAPPER
383 $\uparrow \sigma$	384 2	385 9.11 ± 0.53	386 12.93 ± 0.75	387 33.14 ± 0.22	388 57.77 ± 0.81	389 62.43 ± 0.46
	384 4	385 10.44 ± 0.77	386 19.94 ± 0.47	387 40.19 ± 0.55	388 83.32 ± 0.24	389 85.17 ± 0.10
	384 8	385 9.33 ± 0.54	386 25.46 ± 1.57	387 72.44 ± 0.24	388 91.12 ± 0.08	389 91.08 ± 0.09
386 $\uparrow \mu$	387 2	388 9.11 ± 0.53	389 10.63 ± 0.34	390 33.14 ± 0.22	391 57.77 ± 0.81	392 63.06 ± 0.47
	387 4	388 10.44 ± 0.77	389 18.13 ± 0.71	390 40.19 ± 0.55	391 83.32 ± 0.24	392 85.35 ± 0.06
	387 8	388 9.33 ± 0.54	389 51.33 ± 1.21	390 72.44 ± 0.24	391 91.12 ± 0.08	392 91.02 ± 0.05
388 $\uparrow \mu + \sigma$	389 2	390 9.11 ± 0.53	391 10.45 ± 0.16	392 33.14 ± 0.22	393 57.77 ± 0.81	394 63.02 ± 0.55
	389 4	390 10.44 ± 0.77	391 18.55 ± 0.68	392 40.19 ± 0.55	393 83.32 ± 0.24	394 85.18 ± 0.07
	389 8	390 9.33 ± 0.54	391 51.31 ± 1.29	392 72.44 ± 0.24	393 91.12 ± 0.08	394 91.12 ± 0.07
390 RANDOM-SELECTION	391 2	392 9.11 ± 0.53	393 9.80 ± 0.00	394 33.14 ± 0.22	395 57.77 ± 0.81	396 64.84 ± 0.16
	391 4	392 10.44 ± 0.77	393 17.35 ± 0.27	394 40.19 ± 0.55	395 83.32 ± 0.24	396 85.45 ± 0.06
	391 8	392 9.33 ± 0.54	393 9.23 ± 0.64	394 72.44 ± 0.24	395 91.12 ± 0.08	396 90.80 ± 0.09

393
 394 **Ablation on Budgeting.** We first conducted an ablation study on the MNIST dataset in which four
 395 different Budgeting criterias were tested.

396 In **Budgeting using High Variance** ($\uparrow \sigma$) we sampled 5% weights with ‘High Variance’ from
 397 the posterior distributions (parameters: μ, σ) of the whole model and transformed them to belief
 398 posteriors using Epistemic Wrapper. The results are shown in Table 1, where ‘MLP size’ is the
 399 number of hidden units in the single hidden layer of the model. Since inference in our methodology
 400 is done using INNs, we compare our results with those of INN (taken as a baseline). The results
 401 shows that using the wrapper improves the quality of the weights initialization with respect to the
 402 INN baseline. For instance, an MLP with 32 hidden units and weights randomly initialized achieved
 403 an accuracy of 10.37% on the test data, while for our wrapper the test accuracy was 50.20%.

404 **Budgeting using High Mean** ($\uparrow \mu$) is another strategy in which we sample and ‘wrap’ the 5%
 405 weights with ‘High Mean’ from the posterior distributions. From the results shown in Table 1, it can
 406 be seen that ‘High Mean’ performs better for MLP size (no hidden units) = 8.

407 **In Budgeting using High Mean and High Variance** ($\uparrow (\mu, \sigma)$) we rank the parameters by computing
 408 a combined score, defined as the sum of the mean and variance of their posterior distributions:
 409 $\text{combined_score} = \mu + \sigma$. This acts as a proxy for an upper bound of the posterior distribution,
 410 allowing us to prioritize parameters that are either highly informative (high mean) or uncertain (high
 411 variance). We then wrap these top 5% weights using Epi-wrapper. The results are shown in Table 1.
 412 This strategy allows us to selectively wrap the most influential and uncertain parameters, ensuring that
 413 the transformation captures meaningful epistemic uncertainty. However, this approach also imposes
 414 a strict constraint on the selection process, as only weights satisfying both conditions are chosen,
 415 which may limit flexibility in certain scenarios.

416 **Budgeting using Random Selection** (μ, σ) is done by randomly selecting 5% weights from the
 417 baseline BNN and extract belief posteriors using the wrapper. Table 1 shows that the results are worse
 418 than with other strategies. This is due to the fact that random sampling, while giving us an unbiased
 419 selection of posterior weights, may miss those posterior distributions with high uncertainty that can
 420 be improved using our wrapping approach.

421 **Note:** The lower MNIST and Fashion-MNIST accuracies come from the very small Bayesian
 422 backbone we used: a single-layer variational MLP with only 8 hidden units.

423 4.2 FINE-TUNING

424 We performed the fine-tuning of the models, the INN (baseline) and Epi-Wrapper (ours), on the
 425 training data. The results are shown in Table 1 and Table 2. In comparison to the INN and BNN
 426 baselines, our model performs well as the wrapping of weights acts as an initialization strategy in
 427 fine-tuning. The details of Fine-Tuning are presented in Appendix Section C.2

428 4.3 iD AND OoD EXPERIMENTAL EVALUATION

429 **To evaluate how well the model captures epistemic uncertainty, we consider both *in-distribution***
 430 **(iD) and *out-of-distribution* (OoD) datasets. The iD dataset corresponds to the standard test split of**

432
 433 Table 2: Classification accuracies of INN and Epi-Wrapper models before and after fine-tuning across
 434 multiple datasets and Bayesian backbones (MLP, LeNet-5, ResNet-18, VGG-16) with BNNF and
 435 BNNR baselines. Reported values are mean \pm standard deviation over 15 runs.
 436

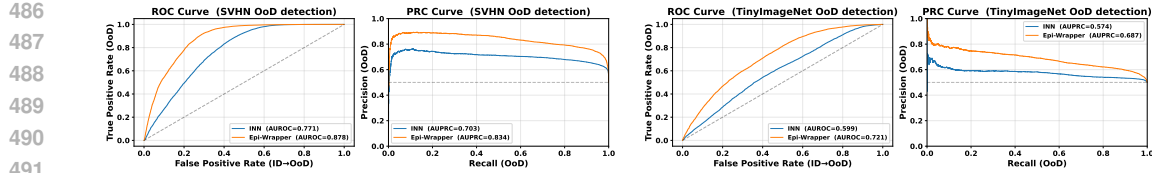
437 DATASET	BACKBONE	# PARAMS	BASELINE	BNN	BEFORE FINE-TUNING		AFTER FINE-TUNING	
					438 INN	EPI-WRAPPER	439 INN	EPI-WRAPPER
439 MNIST	MLP	12.7K	BNNF	72.44 \pm 0.24	9.33 \pm 0.54	51.33 \pm 1.21	91.07 \pm 0.08	91.12 \pm 0.05
	FASHION-MNIST	MLP	BNNF	58.91 \pm 0.24	8.57 \pm 1.03	26.93 \pm 1.44	82.41 \pm 0.19	82.45 \pm 0.10
	440 CIFAR-10	LENET-5	BNNF	47.26 \pm 0.24	9.80 \pm 0.18	42.34 \pm 0.12	45.92 \pm 0.36	47.89 \pm 0.01
			BNNR	47.09 \pm 0.13	9.80 \pm 0.18	42.45 \pm 0.20	45.92 \pm 0.36	47.99 \pm 0.09
			441 RESNET-18	9.82M	BNNF	86.79 \pm 0.21	10.38 \pm 0.17	20.11 \pm 0.02
	442 VGG-16	30.24M	BNNR	85.83 \pm 0.30	10.38 \pm 0.17	26.71 \pm 0.11	87.07 \pm 0.23	89.96 \pm 0.07
			BNNF	87.39 \pm 0.67	9.56 \pm 0.33	65.83 \pm 0.06	87.99 \pm 0.30	88.70 \pm 0.06
			BNNR	88.29 \pm 0.87	9.56 \pm 0.33	50.31 \pm 0.08	87.99 \pm 0.30	89.87 \pm 0.09
444 CIFAR-100	9.8M	30.24M	BNNF	67.38 \pm 0.92	1.23 \pm 0.11	13.29 \pm 0.51	62.70 \pm 0.19	67.41 \pm 0.33
			BNNR	67.47 \pm 0.45	1.23 \pm 0.11	19.48 \pm 0.05	62.70 \pm 0.19	67.49 \pm 0.32
			BNNF	65.48 \pm 0.85	0.96 \pm 0.04	23.32 \pm 0.04	60.10 \pm 1.04	65.55 \pm 0.13
			BNNR	66.59 \pm 0.36	0.96 \pm 0.04	16.11 \pm 0.05	60.10 \pm 1.04	66.63 \pm 0.19

447 Table 3: OoD detection results (AUROC, AUPRC, and mean entropy) for INN (baseline) and Epi-
 448 Wrapper (ours). Models are trained on in-distribution (iD) datasets (MNIST, CIFAR-10, CIFAR-100)
 449 and evaluated on their corresponding out-of-distribution (OoD) datasets: MNIST \rightarrow Fashion-MNIST,
 450 CIFAR-10 \rightarrow SVHN, CIFAR-100 \rightarrow TinyImageNet. Results are reported for BNNF and BNNR
 451 baselines using MLP, LeNet-5, ResNet-18, and VGG-16 backbones.

454 DATASET	BACKBONE	# PARAMS	BASELINE	AUROC (\uparrow)		AUPRC (\uparrow)		ENTROPY (\uparrow)		
				455 INN	EPI-WRAPPER	456 INN	EPI-WRAPPER	457 INN	EPI-WRAPPER	
MNIST	MLP	12.7K	BNNF	0.532 \pm 0.011	0.667 \pm 0.009	0.895 \pm 0.035	0.912 \pm 0.055	0.201 \pm 0.044	0.287 \pm 0.067	
456 FASHION-MNIST	457 MLP	12.7K	BNNF	0.605 \pm 0.041	0.690 \pm 0.076	0.855 \pm 0.015	0.922 \pm 0.015	0.247 \pm 0.030	0.299 \pm 0.019	
				458 BNNR	0.678 \pm 0.006	0.781 \pm 0.009	0.620 \pm 0.048	0.751 \pm 0.003	1.763 \pm 0.010	1.995 \pm 0.045
				459 BNNR	0.678 \pm 0.006	0.781 \pm 0.009	0.620 \pm 0.004	0.728 \pm 0.007	1.763 \pm 0.010	2.005 \pm 0.013
	460 CIFAR-10	166.3K	BNNF	0.678 \pm 0.006	0.749 \pm 0.001	0.724 \pm 0.019	0.799 \pm 0.008	0.569 \pm 0.035	0.659 \pm 0.034	
				461 BNNR	0.806 \pm 0.014	0.859 \pm 0.003	0.724 \pm 0.019	0.824 \pm 0.008	0.569 \pm 0.035	0.764 \pm 0.021
				462 RESNET-18	0.806 \pm 0.014	0.861 \pm 0.005	0.796 \pm 0.014	0.801 \pm 0.015	0.606 \pm 0.058	0.611 \pm 0.046
463 CIFAR-100	464 VGG-16	30.24M	BNNF	0.849 \pm 0.011	0.850 \pm 0.011	0.796 \pm 0.014	0.799 \pm 0.015	0.601 \pm 0.034		
				465 BNNR	0.849 \pm 0.011	0.856 \pm 0.010	0.796 \pm 0.014	0.606 \pm 0.058	0.601 \pm 0.034	
	466 RESNET-18	9.8M	BNNF	0.616 \pm 0.031	0.705 \pm 0.089	0.688 \pm 0.005	0.770 \pm 0.040	1.908 \pm 0.043	1.912 \pm 0.067	
				467 BNNR	0.616 \pm 0.031	0.690 \pm 0.019	0.688 \pm 0.005	0.710 \pm 0.029	1.908 \pm 0.043	1.920 \pm 0.075

468 the training distribution (e.g. MNIST, CIFAR-10), while the OoD dataset consists of samples that
 469 differ significantly from the training set (e.g. Fashion-MNIST for MNIST-trained models, SVHN or
 470 TinyImageNet for CIFAR-trained models). A model with strong epistemic uncertainty should assign
 471 higher entropy to OoD samples. Therefore, we analyse predictive entropy, calibration metrics, and
 472 OoD detection performance across both types of datasets.

473 **Uncertainty via Predictive Entropy and OoD Detection.** Our interval network outputs, for each
 474 input x , a pair of class–logit vectors $(\ell^L, \ell^U) \in \mathbb{R}^C$ representing lower and upper logits. We form a sin-
 475 gle logit vector by midpoint aggregation $\tilde{\ell} = \frac{1}{2}(\ell^L + \ell^U)$, and convert to class probabilities with tem-
 476 perature T (default $T=1$) via $p_T(y=c|x) = \text{softmax}(\tilde{\ell}/T)_c$. We quantify predictive uncertainty us-
 477 ing the (Shannon) predictive entropy $H_T(x) = -\sum_{c=1}^C p_T(y=c|x) \log p_T(y=c|x)$. For the out-
 478 of-distribution (OoD) set \mathcal{D}_{ood} we report the mean OoD entropy $\overline{H}_T^{\text{OoD}} = |\mathcal{D}_{\text{ood}}|^{-1} \sum_{x \in \mathcal{D}_{\text{ood}}} H_T(x)$,
 479 and analogously compute the mean entropy on the in-distribution (ID) test set. We further assess
 480 OoD separability by using $H_T(x)$ as a scalar score (higher implies more OoD-like). Concatenating
 481 the ID and OoD scores with labels $\{0, 1\}$ (ID as 0, OoD as 1), we compute the area under the ROC
 482 curve (AUROC) and the area under the precision–recall curve (AUPRC). Thus, in our experiments
 483 *entropy is the uncertainty measure*: higher entropy indicates greater predictive uncertainty and is
 484 used directly to evaluate both calibration (through mean entropy and NLL/ECE) and OoD detection
 485 (via AUROC/AUPRC). Table 3 shows that Epi-Wrapper consistently improves OoD detection per-
 486 formance across all datasets and architectures. In particular, it achieves higher AUROC, AUPRC, and
 487 entropy scores compared to the INN baseline, demonstrating stronger separability between iD and
 488 OoD samples. This trend is further confirmed by the ROC and PRC curves in Figure 5a and Figure 5b,



486
487
488
489
490
491
492 (a) ROC and PRC curves for iD CIFAR-10
493 vs. SVHN OoD detection using ResNet-18 with
494 BNNR (Molchanov et al., 2017).
495
496
497
498
499
500 (b) ROC and PRC curves for iD CIFAR-100 vs.
501 TinyImageNet OoD detection using VGG-16 with
502 BNNR (Molchanov et al., 2017).

500 Figure 5: ROC and PRC results for OoD detection on SVHN and TinyImageNet benchmarks using
501 INN and Epi-Wrapper. The curves illustrate performance trade-offs under entropy-based scoring,
502 with AUROC and AUPRC values reported in the legends.

500 where Epi-Wrapper outperforms the INN baseline. Additional ROC/PRC results are presented in
501 Section C.4, and calibration results (NLL/ECE) are reported in Appendix C.5.

503 4.4 ADDITIONAL RESULTS AND DETAILS IN APPENDIX

504 We summarize the contents of the Appendix in this section. Appendix A provides theoretical
505 background concepts, including Belief functions, Dirichlet distributions, and the functionality of
506 Interval Neural Networks (INNs). Appendix B contains implementation details, dataset descriptions,
507 and Bayesian baseline setups. It also specifies the backbone architectures (MLP, LeNet-5, ResNet-18,
508 and VGG-16), BNN training procedures, and computational costs. Appendix C presents additional
509 ablation studies, including distributional choices over the simplex, the effect of budget set size, and
510 the effect of the number of closed intervals. It also contains details on fine-tuning large-scale models,
511 hyperparameter settings, ROC and PRC computation procedures, and results on calibration and
512 likelihood evaluation. Appendix D discusses modeling epistemic uncertainty in parameter space
513 versus target space. Appendix E outlines a preliminary idea for extending Epi-Wrapper to regression
514 tasks.

515 5 CONCLUSION AND FUTURE DIRECTIONS

516 This paper introduces *Epistemic Wrapper*, a methodology that extends higher-order uncertainty
517 representation into the parameter space of neural networks. Building on BNNs, it transforms their
518 outputs into belief-function posteriors, enabling richer and more expressive quantification of epistemic
519 uncertainty. The method is robust, efficient, and applicable across architectures, with experiments on
520 four benchmark datasets showing consistent improvements in uncertainty estimation. A limitation is
521 that Epi-Wrapper’s performance depends on the quality of the underlying BNN, as poorly trained
522 or high-variance models may yield degraded belief-function outputs. As future work, we aim to
523 integrate Epistemic Wrapper with Bayesian Neural Operators for structured uncertainty quantification
524 in function space, particularly for complex physical systems governed by PDEs. Another direction is
525 to use the wrapped weights to construct predictive random sets in the target space, advancing reliable
526 uncertainty-aware learning.

527 530 REFERENCES

531 Moloud Abdar, Farhad Pourpanah, Sadiq Hussain, Dana Rezazadegan, Li Liu, Mohammad
532 Ghavamzadeh, Paul Fieguth, Xiaochun Cao, Abbas Khosravi, U Rajendra Acharya, et al. A
533 review of uncertainty quantification in deep learning: Techniques, applications and challenges.
534 *Information Fusion*, 76:243–297, 2021.

535 Gustaf Ahdritz, Aravind Gollakota, Parikshit Gopalan, Charlotte Peale, and Udi Wieder. Provable
536 uncertainty decomposition via higher-order calibration. *arXiv preprint arXiv:2412.18808*, 2024.

537 David M Blei, Alp Kucukelbir, and Jon D McAuliffe. Variational inference: A review for statisticians.
538 *Journal of the American statistical Association*, 112(518):859–877, 2017.

540 Charles Blundell, Julien Cornebise, Koray Kavukcuoglu, and Daan Wierstra. Weight uncertainty
 541 in neural network. In *Proceedings of the International Conference on Machine Learning*, pp.
 542 1613–1622. PMLR, 2015.

543 Michele Caprio, Maryam Sultana, Eleni Elia, and Fabio Cuzzolin. Credal learning theory. *arXiv*
 544 *preprint arXiv:2402.00957*, 2024.

545 Matthew Albert Chan, Maria J. Molina, and Christopher Metzler. Estimating epistemic and aleatoric
 546 uncertainty with a single model. In *The Thirty-eighth Annual Conference on Neural Information
 547 Processing Systems*, 2024. URL <https://openreview.net/forum?id=WPxa6OcIdg>.

548 Bertrand Charpentier, Daniel Zügner, and Stephan Günnemann. Posterior network: Uncertainty
 549 estimation without ood samples via density-based pseudo-counts. *Advances in neural information
 550 processing systems*, 33:1356–1367, 2020.

551 Fabio Cuzzolin. Geometry of Upper Probabilities. In *ISIPTA*, pp. 188–203, 2003.

552 Fabio Cuzzolin. Geometry of Dempster’s rule of combination. *IEEE Transactions on Systems, Man
 553 and Cybernetics part B*, 34(2):961–977, 2004.

554 Fabio Cuzzolin. Two new Bayesian approximations of belief functions based on convex geometry.
 555 *IEEE Transactions on Systems, Man, and Cybernetics - Part B*, 37(4):993–1008, 2007.

556 Fabio Cuzzolin. On the credal structure of consistent probabilities. In *European Workshop on Logics
 557 in Artificial Intelligence*, pp. 126–139. Springer, 2008a.

558 Fabio Cuzzolin. A geometric approach to the theory of evidence. *IEEE Transactions on Systems,
 559 Man, and Cybernetics, Part C (Applications and Reviews)*, 38(4):522–534, 2008b.

560 Fabio Cuzzolin. Complexes of outer consonant approximations. In *Proceedings of the 10th Eu-
 561 ropean Conference on Symbolic and Quantitative Approaches to Reasoning with Uncertainty
 562 (ECSQARU’09)*, pp. 275–286, 2009.

563 Fabio Cuzzolin. Credal semantics of Bayesian transformations in terms of probability intervals. *IEEE
 564 Transactions on Systems, Man, and Cybernetics, Part B: Cybernetics*, 40(2):421–432, 2010a.

565 Fabio Cuzzolin. Geometric conditioning of belief functions. *Proceedings of BELIEF*, 10, 2010b.

566 Fabio Cuzzolin. The geometry of consonant belief functions: simplicial complexes of necessity
 567 measures. *Fuzzy Sets and Systems*, 161(10):1459–1479, 2010c.

568 Fabio Cuzzolin. On consistent approximations of belief functions in the mass space. In *European
 569 Conference on Symbolic and Quantitative Approaches to Reasoning and Uncertainty*, pp. 287–298.
 570 Springer, 2011.

571 Fabio Cuzzolin. Lp consonant approximations of belief functions. *IEEE Transactions on Fuzzy
 572 Systems*, 22(2):420–436, April 2014a.

573 Fabio Cuzzolin. *Belief functions: theory and applications*. Springer, 2014b.

574 Fabio Cuzzolin. Generalised max entropy classifiers. In Sébastien Destercke, Thierry Denœux, Fabio
 575 Cuzzolin, and Arnaud Martin (eds.), *Belief Functions: Theory and Applications*, pp. 39–47, Cham,
 576 2018a. Springer International Publishing.

577 Fabio Cuzzolin. Visions of a generalized probability theory. *arXiv preprint arXiv:1810.10341*, 2018b.

578 Fabio Cuzzolin. *The geometry of uncertainty: The geometry of imprecise probabilities*. Springer
 579 Nature, 2020.

580 Fabio Cuzzolin. Uncertainty measures: The big picture. *arXiv preprint arXiv:2104.06839*, 2021.

581 Fabio Cuzzolin. Uncertainty measures: A critical survey. *Information Fusion*, pp. 102609, 2024.

582 Fabio Cuzzolin. Lp consonant approximations of belief functions in the mass space. In *Proceedings of
 583 the 7th International Symposium on Imprecise Probability: Theory and Applications (ISIPTA’11)*,
 584 July 2011.

594 Fabio Cuzzolin and Ruggero Frezza. Geometric analysis of belief space and conditional subspaces.
 595 In *ISIPTA*, pp. 122–132, 2001.
 596

597 Fabio Cuzzolin and Wenjua Gong. Belief modeling regression for pose estimation. In *Proceedings of*
 598 *the 16th International Conference on Information Fusion*, pp. 1398–1405, 2013.

599 Arthur P. Dempster. Upper and lower probabilities induced by a multivalued mapping. *The Annals of*
 600 *Mathematical Statistics*, 38(2):325–339, 1967. doi: 10.1214/aoms/1177698950.
 601

602 Stanislav Fort and Stanislaw Jastrzebski. Large scale structure of neural network loss landscapes.
 603 *Advances in Neural Information Processing Systems*, 32, 2019.

604 Dominik Fuchsgruber, Tom Wollschläger, and Stephan Günnemann. Energy-based epistemic uncer-
 605 tainty for graph neural networks. In *The Thirty-eighth Annual Conference on Neural Information*
 606 *Processing Systems*, 2024. URL <https://openreview.net/forum?id=6vNPtWH1Q>.
 607

608 Yarin Gal and Zoubin Ghahramani. Dropout as a Bayesian approximation: Representing model
 609 uncertainty in deep learning. In *Proceedings of the International Conference on Machine Learning*,
 610 pp. 1050–1059. PMLR, 2016.

611 Andrew Gelman, John B Carlin, Hal S Stern, David B Dunson, Aki Vehtari, and Donald B Rubin.
 612 *Bayesian Data Analysis*. CRC press, 2013.
 613

614 Wenjuan Gong and Fabio Cuzzolin. A belief-theoretical approach to example-based pose estimation.
 615 *IEEE Transactions on Fuzzy Systems*, 26(2):598–611, 2017.

616 Sebastian G Gruber and Florian Buettner. Uncertainty estimates of predictions via a general bias-
 617 variance decomposition. *arXiv preprint arXiv:2210.12256*, 2022.

618 Kaiming He, Xiangyu Zhang, Shaoqing Ren, and Jian Sun. Deep residual learning for image
 619 recognition. In *Proceedings of the IEEE conference on computer vision and pattern recognition*,
 620 pp. 770–778, 2016.

621 Timothy Hickey, Qun Ju, and Maarten H Van Emden. Interval arithmetic: From principles to
 622 implementation. *Journal of the ACM (JACM)*, 48(5):1038–1068, 2001.

623

624 Matthew D Hoffman, Andrew Gelman, et al. The No-U-Turn sampler: Adaptively setting path
 625 lengths in Hamiltonian Monte Carlo. *J. Mach. Learn. Res.*, 15(1):1593–1623, 2014.

626

627 Paul Hofman, Yusuf Sale, and Eyke Hüllermeier. Quantifying aleatoric and epistemic uncertainty: A
 628 credal approach. In *ICML 2024 Workshop on Structured Probabilistic Inference \& Generative*
 629 *Modeling*, 2024.

630

631 J. R. M. Hosking. L-moments: Analysis and estimation of distributions using linear combinations of
 632 order statistics. *Journal of the Royal Statistical Society: Series B (Methodological)*, 52(1):105–124,
 633 12 2018. doi: 10.1111/j.2517-6161.1990.tb01775.x.

634

635 Eyke Hüllermeier and Willem Waegeman. Aleatoric and epistemic uncertainty in machine learning:
 636 An introduction to concepts and methods. *Machine Learning*, 110(3):457–506, 2021.

637

638 Laurent Valentin Jospin, Hamid Laga, Farid Boussaid, Wray Buntine, and Mohammed Bennamoun.
 639 Hands-on Bayesian neural networks—A tutorial for deep learning users. *IEEE Computational*
Intelligence Magazine, 17(2):29–48, 2022.

640

641 Mira Juergens, Nis Meinert, Viktor Bengs, Eyke Hüllermeier, and Willem Waegeman. Is epistemic
 642 uncertainty faithfully represented by evidential deep learning methods? In *Forty-first International*
Conference on Machine Learning, 2024. URL <https://openreview.net/forum?id=mxjB0L1gpt>.
 643

644 LS Kim. Understanding the difficulty of training deep feedforward neural networks xavier. In
 645 *Proceedings of the International Joint Conference on Neural Networks*, volume 2, 1993.
 646

647 Diederik P Kingma and Max Welling. Auto-encoding variational Bayes. *arXiv preprint*
arXiv:1312.6114, 2013.

648 Nikita Kotelevskii, Vladimir Kondratyev, Martin Takáč, Eric Moulines, and Maxim Panov. From risk
 649 to uncertainty: Generating predictive uncertainty measures via bayesian estimation. *arXiv preprint*
 650 *arXiv:2402.10727*, 2024.

651

652 Alex Krizhevsky. Learning multiple layers of features from tiny images. Technical report, Technical
 653 Report, Computer Science Department, University of Toronto, 2009a.

654 Alex Krizhevsky. Learning multiple layers of features from tiny images. Technical re-
 655 port, University of Toronto, 2009b. URL <http://www.cs.toronto.edu/~kriz/learning-features-2009-TR.pdf>.

656

657 Antonis Lambrou, Harris Papadopoulos, and Alex Gammerman. Reliable confidence measures for
 658 medical diagnosis with evolutionary algorithms. *IEEE Transactions on Information Technology in*
 659 *Biomedicine*, 15(1):93–99, 2010.

660

661 Yann LeCun. The MNIST database of handwritten digits. <http://yann.lecun.com/exdb/mnist/>, 1998.

662

663 Yann LeCun, Léon Bottou, Yoshua Bengio, and Patrick Haffner. Gradient-based learning applied to
 664 document recognition. *Proceedings of the IEEE*, 86(11):2278–2324, 1998.

665

666 Isaac Levi. *The enterprise of knowledge: An essay on knowledge, credal probability, and chance*.
 667 MIT press, 1980.

668

669 Xixun Lin, Wenxiao Zhang, Fengzhao Shi, Chuan Zhou, Lixin Zou, Xiangyu Zhao, Dawei Yin,
 670 Shirui Pan, and Yanan Cao. Graph neural stochastic diffusion for estimating uncertainty in node
 671 classification. In *Forty-first International Conference on Machine Learning*, 2024.

672

673 Jeremiah Liu, Zi Lin, Shreyas Padhy, Dustin Tran, Tania Bedrax Weiss, and Balaji Lakshminarayanan.
 674 Simple and principled uncertainty estimation with deterministic deep learning via distance aware-
 675 ness. *Advances in Neural Information Processing Systems*, 33:7498–7512, 2020.

676

677 Zhun-Ga Liu, Yu Liu, Jean Dezert, and Fabio Cuzzolin. Evidence combination based on credal belief
 678 redistribution for pattern classification. *IEEE Transactions on Fuzzy Systems*, 28(4):618–631,
 2019.

679

680 Andrey Malinin, Bruno Mlozoeniec, and Mark Gales. Ensemble distribution distillation. *arXiv*
 681 *preprint arXiv:1905.00076*, 2019.

682

683 Shireen Kudukkil Manchingal and Fabio Cuzzolin. Epistemic deep learning. *arXiv preprint*
 684 *arXiv:2206.07609*, 2022.

685

686 Shireen Kudukkil Manchingal, Muhammad Mubashar, Kaizheng Wang, Keivan Shariatmadar, and
 687 Fabio Cuzzolin. Random-set convolutional neural network (rs-cnn) for epistemic deep learning.
 688 *arXiv preprint arXiv:2307.05772*, 2023.

689

690 Shireen Kudukkil Manchingal, Muhammad Mubashar, Kaizheng Wang, and Fabio Cuzzolin. A
 691 unified evaluation framework for epistemic predictions, 2025a. URL <https://arxiv.org/abs/2501.16912>.

692

693 Shireen Kudukkil Manchingal, Muhammad Mubashar, Kaizheng Wang, Keivan Shariatmadar, and
 694 Fabio Cuzzolin. Random-set neural networks. In *The Thirteenth International Conference on Learn-
 695 ing Representations*, 2025b. URL <https://openreview.net/forum?id=pdjikivCch>.

696

697 Dmitry Molchanov, Arsenii Ashukha, and Dmitry Vetrov. Variational dropout sparsifies deep neural
 698 networks. In *Proceedings of the International Conference on Machine Learning*, pp. 2498–2507.
 699 PMLR, 2017.

700

701 Giorgio Morales and John Sheppard. Adaptive sampling to reduce epistemic uncertainty using
 702 prediction interval-generation neural networks. *Proceedings of the AAAI Conference on Artificial
 Intelligence*, Feb. 2025.

703 Radford M Neal et al. MCMC using Hamiltonian dynamics. *Handbook of Markov Chain Monte
 Carlo*, 2(11):2, 2011.

702 Kazuki Osawa, Siddharth Swaroop, Anirudh Jain, Runa Eschenhagen, Richard E. Turner, Rio Yokota,
 703 and Mohammad Emtiyaz Khan. Practical deep learning with bayesian principles. *arXiv preprint*
 704 *arXiv:1906.02506*, 2019.

705 Yusuf Sale, Michele Caprio, and Eyke Höllermeier. Is the volume of a credal set a good measure for
 706 epistemic uncertainty? In *Uncertainty in Artificial Intelligence*, pp. 1795–1804. PMLR, 2023.

708 Murat Sensoy, Lance Kaplan, and Melih Kandemir. Evidential deep learning to quantify classification
 709 uncertainty. *Advances in neural information processing systems*, 31, 2018.

710 Glenn Shafer. *A mathematical theory of evidence*, volume 42. Princeton university press, 1976.

712 Karen Simonyan and Andrew Zisserman. Very deep convolutional networks for large-scale image
 713 recognition. In *International Conference on Learning Representations (ICLR)*, 2015.

715 Philippe Smets. The transferable belief model and other interpretations of Dempster–Shafer’s model.
 716 In P. P. Bonissone, M. Henrion, L. N. Kanal, and J. F. Lemmer (eds.), *Uncertainty in Artificial*
 717 *Intelligence*, volume 6, pp. 375–383. North-Holland, Amsterdam, 1991.

718 Philippe Smets. Belief functions on real numbers. *International Journal of Approximate Reasoning*,
 719 40(3):181–223, 2005.

721 Andrew Stirn, Tony Jebara, and David A Knowles. A new distribution on the simplex with auto-
 722 encoding applications. In *Advances in Neural Information Processing Systems*, 2019. URL
 723 <https://arxiv.org/abs/1905.12052>. arXiv:1905.12052.

724 Puja Trivedi, Mark Heimann, Rushil Anirudh, Danai Koutra, and Jayaraman J. Thiagarajan. Accurate
 725 and scalable estimation of epistemic uncertainty for graph neural networks. In *The Twelfth*
 726 *International Conference on Learning Representations*, 2024. URL <https://openreview.net/forum?id=ZL6yd6N1S2>.

728 Kaizheng Wang, Fabio Cuzzolin, Keivan Shariatmadar, David Moens, and Hans Hallez. Credal
 729 wrapper of model averaging for uncertainty estimation on out-of-distribution detection. *arXiv*
 730 *preprint arXiv:2405.15047*, 2024a.

732 Kaizheng Wang, Fabio Cuzzolin, Keivan Shariatmadar, David Moens, Hans Hallez, et al. Credal deep
 733 ensembles for uncertainty quantification. *Advances in Neural Information Processing Systems*, 37:
 734 79540–79572, 2024b.

735 Kaizheng Wang, Keivan Shariatmadar, Shireen Kudukkil Manchingal, Fabio Cuzzolin, David Moens,
 736 and Hans Hallez. Creinns: Credal-set interval neural networks for uncertainty estimation in
 737 classification tasks. *Neural Networks*, pp. 107198, 2025.

739 Larry A. Wasserman. Belief functions and statistical inference. *Canadian Journal of Statistics*, 18(3):
 740 183–196, 1990.

741 Yeming Wen, Paul Vicol, Jimmy Ba, Dustin Tran, and Roger Grosse. Flipout: Efficient pseudo-
 742 independent weight perturbations on mini-batches. In *Proceedings of the International Conference*
 743 *on Learning Representations*, 2018. URL <https://openreview.net/forum?id=rJNpifWAb>.

746 Han Xiao, Kashif Rasul, and Roland Vollgraf. Fashion-mnist: a novel image dataset for benchmarking
 747 machine learning algorithms. *arXiv preprint arXiv:1708.07747*, 2017.

748

749

A THEORETICAL BACKGROUND CONCEPTS

750

751

A.1 BELIEF FUNCTIONS

752

753 Belief functions Cuzzolin (2014b; 2018b), grounded in the mathematical framework of random sets,
 754 were initially introduced by Dempster (Dempster, 1967) and later formalized by Shafer (Shafer,
 755 1976) as an alternative model for subjective belief to Bayesian probability. As mathematical objects,
 they have been extensively studied from an original geometric point of view Cuzzolin & Frezza

(2001); Cuzzolin (2003; 2004; 2008b; 2010c;b). Ways of transforming belief functions into Bayesian probabilities or possibility measures have also been investigated Cuzzolin (2009; 2010a; 2011; 2014a; July 2011; 2007).

In finite domains, such as a collection of classes, belief functions are characterised by a *basic probability assignment* (BPA) (Shafer, 1976), which is a set function $m : 2^\Theta \rightarrow [0, 1]$ satisfying $m(\emptyset) = 0$ and $\sum_{A \subseteq \Theta} m(A) = 1$. The value $m(A)$ is interpreted as the probability mass directly assigned to subset $A \subseteq \Theta$ in a random-set formulation (Smets, 1991). Subsets A of Θ with $m(A) > 0$ are referred to as *focal elements*. Classical belief functions extend the notion of discrete mass functions by assigning normalized, non-negative mass values not only to elements $\theta \in \Theta$ but to subsets of Θ , governed by:

$$m(A) \geq 0, \forall A \subseteq \Theta, \quad \sum_{A \subseteq \Theta} m(A) = 1. \quad (7)$$

The belief function $Bel(A)$ associated with a mass function m is defined as the total mass assigned to all subsets $B \subseteq A$. Conversely, m can be recovered from Bel through Moebius inversion Shafer (1976):

$$Bel(A) = \sum_{B \subseteq A} m(B), \quad m(A) = \sum_{B \subseteq A} (-1)^{|A \setminus B|} Bel(B). \quad (8)$$

This formulation demonstrates that classical probability measures are a special case of belief functions, assigning mass exclusively to singletons.

A.2 DIRICHLET DISTRIBUTION

The Dirichlet distribution is a continuous multivariate probability distribution defined over the $(K - 1)$ simplex:

$$\Delta^{K-1} = \left\{ \mathbf{x} \in \mathbb{R}^K \mid x_i \geq 0, \sum_{i=1}^K x_i = 1 \right\}.$$

It is parameterized by a concentration vector $\alpha = (\alpha_1, \dots, \alpha_K)$ with each $\alpha_i > 0$, and its probability density function is given by:

$$f(x_1, \dots, x_K; \alpha_1, \dots, \alpha_K) = \frac{1}{B(\alpha)} \prod_{i=1}^K x_i^{\alpha_i - 1}, \quad (9)$$

where $B(\alpha)$ is the multivariate Beta function:

$$B(\alpha) = \frac{\prod_{i=1}^K \Gamma(\alpha_i)}{\Gamma\left(\sum_{i=1}^K \alpha_i\right)}.$$

The shape of the Dirichlet distribution is governed by the values of α . Higher values lead to more concentrated distributions around the center of the simplex, while lower values result in more dispersed or sparse distributions. Figure 6 illustrates how different α values affect the distribution over the 2D simplex.

The Dirichlet distribution is widely used in Bayesian statistics, especially for modeling topics in documents and for representing uncertainty Gelman et al. (2013).

A.3 INTERVAL NEURAL NETWORKS (INNs)

Traditional *interval neural networks* use deterministic interval-based inputs, outputs, and parameters (weights and biases) for each node. The forward propagation in the l^{th} layer of INNs is expressed as:

$$\begin{aligned} [\underline{a}, \bar{a}]^l &= \sigma^l([\underline{\omega}, \bar{\omega}]^l \odot [\underline{a}, \bar{a}]^{l-1} \oplus [\underline{b}, \bar{b}]^l) \\ &= [\sigma^l(\underline{\omega} + \underline{b}), \sigma^l(\bar{\omega} + \bar{b})] \text{ with} \\ [\underline{\omega}, \bar{\omega}]^l &= [\underline{\omega}, \bar{\omega}]^l \odot [\underline{a}, \bar{a}]^{l-1}, \end{aligned} \quad (10)$$

where \oplus , \ominus , and \odot represent interval addition, subtraction, and multiplication, respectively (Hickey et al., 2001). The terms $[\underline{a}, \bar{a}]^l$, $[\underline{a}, \bar{a}]^{l-1}$, $[\underline{\omega}, \bar{\omega}]^l$, and $[\underline{b}, \bar{b}]^l$ denote the interval-formed outputs of the

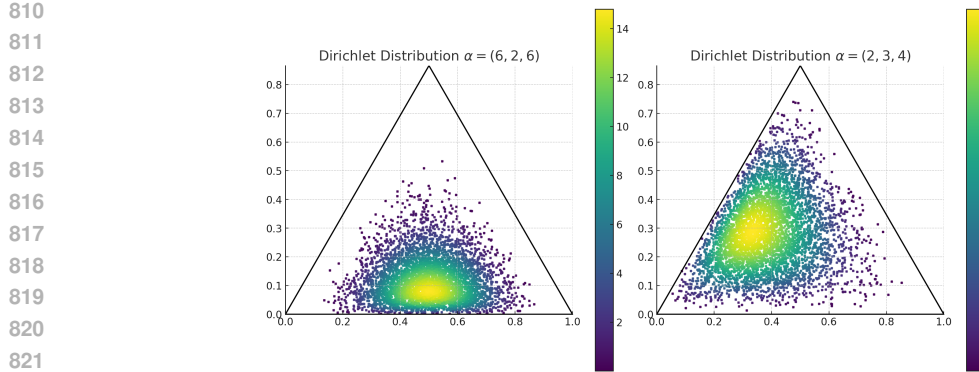


Figure 6: Probability densities of the Dirichlet distribution as functions on the 2D simplex: $\alpha = (6, 2, 6)$ (left), $\alpha = (2, 3, 4)$ (right).

l^{th} and $(l-1)^{th}$ layers, as well as the intervals of weights and biases of the l^{th} layer, respectively. $\sigma^l(\cdot)$ is the activation function of the l^{th} layer, which must be monotonically increasing. The application of interval arithmetic (Hickey et al., 2001) in eq. equation 10 grants INNs the ‘set constraint’ property. Specifically, for any $\mathbf{a}^{l-1} \in [\underline{\mathbf{a}}, \bar{\mathbf{a}}]^{l-1}$, $\boldsymbol{\omega}^l \in [\underline{\boldsymbol{\omega}}, \bar{\boldsymbol{\omega}}]^l$, and $\mathbf{b}^l \in [\underline{\mathbf{b}}, \bar{\mathbf{b}}]^l$, the constraint in eq. equation 11 consistently holds.

$$\mathbf{a}^l = \sigma^l(\boldsymbol{\omega}^l \cdot \mathbf{a}^{l-1} + \mathbf{b}^l) \in [\underline{\mathbf{a}}, \bar{\mathbf{a}}]^l. \quad (11)$$

If $[\underline{\mathbf{a}}, \bar{\mathbf{a}}]$ is non-negative, such as the output of RELU activation, the calculation of $[\underline{\mathbf{o}}, \bar{\mathbf{o}}]$ in eq. equation 10 can be simplified as:

$$\begin{aligned} \underline{\mathbf{o}} &= \min\{\underline{\boldsymbol{\omega}}, \mathbf{0}\} \cdot \bar{\mathbf{a}} + \max\{\underline{\boldsymbol{\omega}}, \mathbf{0}\} \cdot \underline{\mathbf{a}} \\ \bar{\mathbf{o}} &= \max\{\bar{\boldsymbol{\omega}}, \mathbf{0}\} \cdot \bar{\mathbf{a}} + \min\{\bar{\boldsymbol{\omega}}, \mathbf{0}\} \cdot \underline{\mathbf{a}}. \end{aligned} \quad (12)$$

A.4 INTERVAL WEIGHTS FROM WRAPPED POSTERIORS

Dirichlet sampling yields probability vectors on the simplex, not intervals. In our framework, each Dirichlet sample is therefore *mapped* to an interval so that it can be propagated through the Interval Neural Network (INN). Given a Dirichlet sample $\mathbf{x} = (x_1, x_2, x_3)$, we define the corresponding interval weight as

$$[\underline{\boldsymbol{\omega}}, \bar{\boldsymbol{\omega}}] = [\min_k x_k, \max_k x_k].$$

This interval summarises the dispersion encoded by the Dirichlet posterior and fits naturally within the INN’s interval-based forward rules (see Eq. equation 10). These are the *wrapped* weights produced by the Epistemic Wrapper.

For comparison, INNs using *unwrapped* BNN parameters construct interval weights from Gaussian posteriors via

$$\underline{\boldsymbol{\omega}} = \mu - \sigma, \quad \bar{\boldsymbol{\omega}} = \mu + \sigma,$$

which yields a symmetric interval around the mean. Thus, during inference the INN operates with two types of interval weights: (i) Dirichlet-derived intervals for wrapped parameters, and (ii) Gaussian-derived intervals for unwrapped parameters. Aside from the initial interval construction, the forward propagation is identical.

It is important to emphasise that our use of the Dirichlet differs from its classical role in evidential deep learning. There, Dirichlet samples are treated as categorical probability vectors. In our case, the Dirichlet is fitted to mass vectors defined over closed parameter intervals obtained via Möbius inversion. Its domain is therefore a mass function over sets of parameter values, not a categorical sample space. The interval mapping reflects this domain shift: the Dirichlet captures uncertainty over parameter intervals, and each sample yields an interval bound suitable for stable propagation through the INN.

864 **Algorithm 1** Epistemic Wrapper for Parameter-Space Epistemic Uncertainty

865
 866 **Require:** Pretrained BNN with variational posterior $q(\omega)$; posterior samples $\{\omega^{(s)}\}_{s=1}^S$; number of
 867 closed intervals M ; budgeting percentage β .

868 1: **EpistemicWrapper**($q(\omega), \{\omega^{(s)}\}$)
 869 2: Select a subset of weights \mathcal{W} using the budgeting criterion (e.g., high-mean or random)
 870 3: **for** each weight $\omega \in \mathcal{W}$ **do**
 871 4: **(1) Estimate posterior parameters**
 872 5: Compute posterior mean μ and standard deviation σ
 873 6: **(2) Dynamic truncation**
 874 7: $\text{mult} \leftarrow \min(5.0, 1/\sigma)$
 875 8: $a_{\min} = \mu - \text{mult} \cdot \sigma$
 876 9: $a_{\max} = \mu + \text{mult} \cdot \sigma$
 877 10: **(3) Construct closed-interval grid**
 878 11: Discretize $[a_{\min}, a_{\max}]$ into M closed intervals $\{A_i = [a_i, b_i]\}_{i=1}^M$
 879 12: **(4) Compute belief and plausibility**
 880 13: **for** each interval A_i **do**
 881 14: $Pl(A_i) \leftarrow \sup_{\omega \in A_i} q(\omega)$
 882 15: $Bel(A_i) \leftarrow 1 - Pl(A_i^c)$
 883 16: **end for**
 884 17: **(5) Möbius inversion (Belief \rightarrow Mass)**
 885 18: **for** each interval A_i **do**
 886 19: $m(A_i) = \sum_{B \subseteq A_i} (-1)^{|A_i \setminus B|} Bel(B)$
 887 20: **end for**
 888 21: **(6) Normalize mass values**
 889 22: $\tilde{m}_i = m(A_i) / \sum_{j=1}^M m(A_j)$
 890 23: **(7) Project onto 3D simplex**
 891 24: Map $\{\tilde{m}_i\}_{i=1}^M$ to a 3D simplex via barycentric projection
 892 25: **(8) Compute L-moments**
 893 26: Compute weighted first L-moment L_1 and second L-moment L_2
 894 27: **(9) Fit Dirichlet distribution**
 895 28: $\alpha_k = L_{1,k} \left(\frac{L_{1,k}(1-L_{1,k})}{L_{2,k}} - 1 \right), \quad k = 1, 2, 3$
 896 29: Clamp α_k to ensure positivity
 897 30: Store $\alpha_\omega = (\alpha_1, \alpha_2, \alpha_3)$
 898 31: **end for**
 899 32: **return** $\{\text{Dir}(\alpha_\omega)\}_{\omega \in \mathcal{W}}$

900
 901 **B EXPERIMENTAL SETUP**
 902903 **B.1 IMPLEMENTATION DETAILS**
 904

905
 906 All experiments are implemented using the TensorFlow framework (version 2.13.1), with probabilistic
 907 modeling and inference carried out using TensorFlow Probability (TFP) (version 0.21.0). TFP is a
 908 library for statistical analysis and probabilistic reasoning that integrates seamlessly with TensorFlow.
 909 We employed two Bayesian baseline models: ‘BNNR’, which uses Auto-Encoding Variational
 910 Bayes (Kingma & Welling, 2013) with the local re-parameterization trick (Molchanov et al., 2017),
 911 and ‘BNNF’, which leverages the Flipout gradient estimator along with a negative evidence lower
 912 bound (ELBO) loss (Wen et al., 2018). Both baselines are implemented using TFP’s built-in
 913 variational layers and loss functions. Our complete pipeline, including training, inference, and
 914 evaluation of the Epistemic Wrapper is built entirely in TensorFlow 2.13.1 and executed on a machine
 915 equipped with 8× NVIDIA A30 GPUs. For clarity, a full algorithmic description of the Epistemic
 916 Wrapper is provided in Algorithm 1.
 917

918
919

B.2 DATASETS

920
921
922
923
924

We evaluated the performance of the Epistemic Wrapper on four classification benchmarks: MNIST (LeCun, 1998), Fashion-MNIST Xiao et al. (2017), CIFAR-10 (Krizhevsky, 2009a) and CIFAR-100 Krizhevsky (2009b). Following are the details of the iD and OoD datasets.

925
926

B.2.1 iD DATASETS

927
928
929

MNIST dataset comprises 70,000 greyscale images of handwritten digits (0-9), each with a resolution of 28×28 pixels, and is mostly used for classification and pattern recognition tasks due to its simplicity and accessibility.

930
931
932
933

Fashion MNIST serves as a more challenging alternative to MNIST, containing 70,000 greyscale images of fashion items, such as shirts, shoes, and bags, also at same resolution of 28×28 pixels. This dataset provides a greater diversity in texture and structure, making it suitable for evaluating model’s generalization capabilities.

934
935
936
937

CIFAR-10 is a collection of 60,000 color images (split into 50,000 training and 10,000 testing samples) across 10 classes, including animals and vehicles, with each image having a resolution of 32×32 pixels. CIFAR-10 is particularly valuable for assessing models in tasks involving color and more complex spatial patterns.

938
939
940
941
942
943
944

CIFAR-100 consists of 60,000 color images, each of size 32×32 pixels with three RGB channels, divided into 50,000 training images and 10,000 test images. The dataset contains 100 fine-grained classes, with each class having 600 samples, making it a more challenging extension of the CIFAR-10 dataset. Unlike CIFAR-10, which includes only 10 broad categories, CIFAR-100 introduces a hierarchical structure, grouping its 100 classes into 20 superclasses based on semantic similarity.

945
946

B.2.2 OoD DATASETS

947
948
949
950
951
952
953

SVHN (Street View House Numbers) is a real-world image dataset obtained from house numbers captured by Google Street View. It consists of over 600,000 digit images (0-9), cropped from street number plates, with each image being 32×32 pixels in RGB format. Unlike the balanced and object-centric nature of CIFAR datasets, SVHN exhibits high variability in illumination, orientation, and background clutter. It is primarily designed for digit recognition tasks but is widely adopted as an OoD dataset when models are trained on natural object datasets such as CIFAR-10 or CIFAR-100, due to its distinct visual domain.

954
955
956
957
958
959
960
961

TinyImageNet is a subset of the ImageNet dataset constructed for benchmarking under constrained input dimensions. It contains 200 object classes with 500 training images, 50 validation images, and 50 test images per class, leading to a total of 100,000 images. Each image is downsampled to 64×64 pixels, significantly smaller than the original ImageNet resolution. The dataset retains substantial intra-class variation and fine-grained categories. Due to its larger diversity and semantic distance from CIFAR classes, TinyImageNet serves as a strong OoD benchmark for evaluating model robustness and generalization.

962
963

B.3 BAYESIAN BASELINES

964
965
966
967
968
969
970
971

In our current implementation, we employ standard and widely-used VI methods such as Auto-Encoding Variational Bayes with local reparameterization BNNR (Auto-Encoding Variational Bayes (Kingma & Welling, 2013) with the local re-parameterization trick (Molchanov et al., 2017)), and BNNF (Flipout gradient estimator with the negative evidence lower bound loss (Wen et al., 2018)). These provide reliable and efficient posterior approximations and are well-supported in TensorFlow, offering a stable foundation for Bayesian neural network training. The core design of the Epistemic Wrapper is independent of the specific VI family used to approximate the posterior. It operates on sampled posterior weights, and thus can naturally extend to richer VI families. We chose mean-field-based VI families in this initial study for their computational tractability and widespread adoption.

972

B.4 BACKBONES

973

974

975

We utilized four backbone models in our experiments: MLP, LeNet-5 LeCun et al. (1998), ResNet-18 (He et al., 2016), and VGG-16 Simonyan & Zisserman (2015). The architectural details of each backbone are provided below.

978

MLP is composed of an input layer, a single hidden layer and an output layer. The input layer processes the input data with a shape that corresponds to the dimensions of the dataset. For grayscale datasets (MNIST and Fashion MNIST), the input shape is $28 \times 28 \times 1$, and for CIFAR-10 and CIFAR-100, the input shape is $32 \times 32 \times 3$. A flattening layer flattens the input into a single-dimensional vector to be fed to the subsequent dense layers. ‘DenseFlipout Layers’ are implemented using TFP. They approximate the weight posterior distributions using a Flipout Monte Carlo estimator, which reduces the variance of gradient estimates during backpropagation. The first dense layer contains hidden units with ReLU activation, followed by a dropout layer to prevent overfitting. The second dense layer, which acts as the output layer, maps to the number of classes in the dataset.

987

LeNet-5 architecture is adapted into a fully Bayesian framework using variational inference with Flipout layers from TensorFlow Probability. Both convolutional and fully connected layers are replaced with their Flipout-based counterparts. The input shape is dataset dependent: $28 \times 28 \times 1$ for grayscale datasets such as MNIST and Fashion-MNIST, and $32 \times 32 \times 3$ for RGB datasets such as CIFAR-10 and CIFAR-100. The model begins with a ‘Convolution2DFlipout’ layer with 6 filters and a 5×5 kernel, followed by an average pooling layer. This is followed by a second ‘Convolution2DFlipout’ layer with 16 filters and another 5×5 kernel, again followed by average pooling. The output is then flattened and passed through two fully connected variational layers: a ‘DenseFlipout’ layer with 120 units and ReLU activation, followed by a second ‘DenseFlipout’ layer with 84 units. The final classification is performed by a ‘DenseFlipout’ layer with softmax activation and a number of units equal to the number of classes.

988

989

990

991

992

993

994

995

996

997

ResNet-18 model leverages Bayesian Convolutional Neural Networks (Bayesian CNNs) with Flipout and Reparameterization layers from TensorFlow Probability, enabling weight uncertainty modeling. The architecture consists of four main residual blocks, with convolutional layers followed by batch normalization and ReLU activation. The convolutional layers employ Bayesian weight posterior distributions, where the kernel weights follow a Gaussian posterior parameterized by mean and variance. These distributions are constrained using a log-variance regularization technique, ensuring numerical stability. The weight posteriors are sampled using the Mean-Field Variational Inference approach, enabling Bayesian updates during training. The ResNet-18 backbone begins with an initial convolutional layer followed by four residual blocks, each progressively increasing the number of filters from 64 to 512. The residual connections allow gradient flow through the network, ensuring stable training. The final layers include average pooling, flattening, and a fully connected Bayesian dense layer with Flipout, producing the classification logits.

1000

1001

1002

1003

1004

1005

1006

1007

1008

1009

VGG-16 model integrates Bayesian inference into the classical VGG-16 architecture to enable principled uncertainty estimation in deep learning. The standard convolutional layers are replaced with Bayesian Convolutional Neural Networks (Bayesian CNNs) using Convolution2DReparameterization and Convolution2DFlipout layers from TensorFlow Probability. These layers approximate posterior distributions over weights using Mean-Field Variational Inference, ensuring reliable uncertainty quantification. VGG-16 follows a deep convolutional architecture with 16 layers, consisting of multiple stacked convolutional layers with small 3×3 filters, followed by max pooling layers to progressively reduce spatial dimensions. The Bayesian adaptation maintains this structure while introducing posterior weight sampling in convolutional layers, ensuring that the feature extraction process incorporates uncertainty information. Batch normalization and ReLU activation are applied to enhance convergence stability, while Bayesian priors constrain weight posteriors, preventing overconfidence in predictions. The final classification layers include Bayesian fully connected layers with Flipout, which sample weights during inference to produce uncertainty-aware predictions.

1022

1023

1024

1025

BNR vs. BNNF instantiations: Both BNNR and BNNF share the same Bayesian architectures of all above mentioned backbones but differ in their variational inference strategies:

BNNR (Bayesian Neural Network with Reparameterization) uses the Auto-encoding Variational Bayes Kingma & Welling (2013) along with the local reparameterization trick Molchanov et al.

(2017). This variant estimates the evidence lower bound (ELBO) and applies Gaussian posterior sampling locally per activation.

BNNF (Bayesian Neural Network with Flipout) uses the Flipout estimator Wen et al. (2018), which decorrelates the gradient estimates across examples in a mini-batch, leading to lower variance during optimization. BNNF directly applies Flipout-based sampling in both convolutional and dense layers and uses a negative ELBO as the loss function.

These two baselines allow us to evaluate the effectiveness of our Epistemic Wrapper under different stochastic inference regimes.

B.5 TRAINING DETAILS

As a baseline, we use standard variational Bayesian Neural Networks (BNNs) (Blei et al., 2017), starting with a classical Multilayer Perceptron (MLP) architecture. The Bayesian MLP is trained using the Evidence Lower Bound (ELBO) objective, which combines the negative log-likelihood (NLL) with a Kullback-Leibler (KL) divergence regularization term. The NLL is computed via softmax cross-entropy, and the KL divergence measures the distance between the approximate posterior and the prior distributions over the weights. The MLP models are trained for 20 epochs on MNIST and Fashion-MNIST using the Adam optimizer. The Bayesian LeNet-5 is trained under both BNNR and BNNF setups using the same ELBO-based training strategy. Models are trained for 500 epochs on CIFAR-10 with Adam optimizer, batch size 32. We apply standard data augmentation techniques (random horizontal flipping and cropping). For deeper architectures such ResNet-18 and VGG-16, we adopt dataset-specific training schedules. Models trained on CIFAR-10 are trained for 50 epochs, while those trained on CIFAR-100 are trained for 200 epochs. Batch normalization is applied after each convolutional layer. Both BNNR and BNNF variants are implemented using Flipout-compatible variational layers from TensorFlow Probability and are trained from scratch on a single NVIDIA A30 GPU.

B.6 COMPUTATIONAL COST

The computational overhead introduced by the Epistemic Wrapper is modest. The wrapper operates only on a small, selected subset of weights (5% for MLPs and 0.1% for large-scale models), chosen via our posterior-based budgeting criterion. Since the procedure is applied post hoc to sampled BNN weights, it does not interfere with the forward or backward passes of the underlying Bayesian network. Training cost therefore remains unchanged, and the additional runtime appears only during the wrapping stage. **Hardware:** All experiments were conducted on a workstation equipped with CPUs (32 cores, 2.8 GHz) and 8× NVIDIA A30 GPUs (24 GB each). Each experiment was executed on a single GPU. Table 4 reports the total wrapping time for each model–dataset combination. For instance, applying the wrapper to CIFAR-10 with ResNet-18 takes 403–406 seconds on a single NVIDIA A30 GPU. The overhead scales primarily with model size, as expected, but remains practical even for large architectures such as VGG-16. The wrapper therefore maintains compatibility with large-scale BNNs without imposing substantial computational cost.

C EXPERIMENTAL RESULTS

C.1 ADDITIONAL ABLATION STUDIES

Distributional Choices over the Simplex: To assess the modelling choice of using a Dirichlet distribution for belief posteriors representation, we perform an ablation study comparing it to two alternative probability distributions defined over the simplex. The following experiments compare the Dirichlet with a Generalized Dirichlet and a Beta stick-breaking model, evaluating their ability to capture the structure of the normalized masses in the proposed methodology. While any valid Probability Density Function (PDF) defined over the simplex could, in principle, be used to model belief distributions, Dirichlet distributions have consistently demonstrated empirical effectiveness for representing epistemic uncertainty in neural networks Stirn et al. (2019). To assess this modelling choice more critically, we conduct an ablation study comparing the use of three distributions defined on the probability simplex: (i) a standard Dirichlet distribution fitted using the method of L-moments, (ii) a Generalized Dirichlet distribution, and (iii) a Beta stick-breaking model. The Dirichlet distribu-

Table 4: End-to-end runtime of the Epistemic Wrapper on a single NVIDIA A30 GPU. Times correspond to wrapping the selected subset of posterior weights (5% for MLPs and 0.1% for LeNet-5, ResNet-18 and VGG-16). Training time of the underlying BNN is unchanged.

Dataset	Backbone	# Params	Baseline	Budgeting %	Computational Time (Seconds)
MNIST	MLP	12.7K	BNNF	5.0%	17.23
FASHION-MNIST	MLP	12.7K	BNNF	5.0%	17.07
	LENET-5	166.3K	BNNF	0.1%	8.65
			BNNR	0.1%	9.33
CIFAR-10	RESNET-18	9.82M	BNNF	0.1%	403.56
			BNNR	0.1%	405.53
	VGG-16	30.24M	BNNF	0.1%	4003.19
			BNNR	0.1%	4160.05
CIFAR-100	RESNET-18	9.8M	BNNF	0.1%	1304.67
			BNNR	0.1%	1317.49
	VGG-16	30.24M	BNNF	0.1%	4066.00
			BNNR	0.1%	4180.30

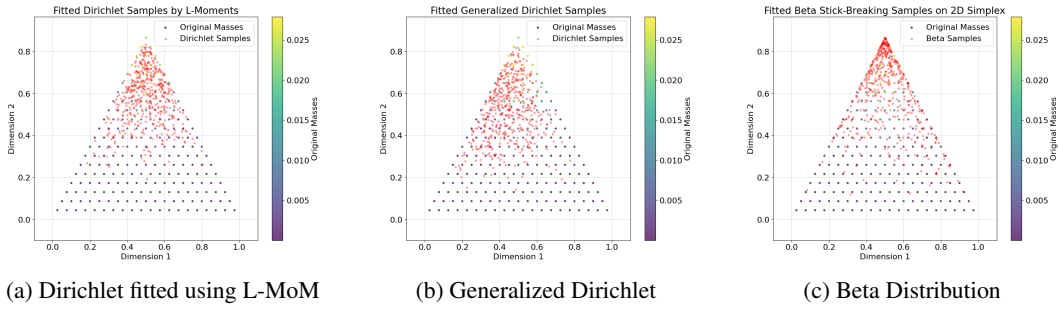


Figure 7: Distributional Choices over the Simplex

tion is used as our baseline because it offers a mathematically simple, symmetric, and interpretable formulation that is widely adopted in evidential deep learning literature. It allows us to encode a single mode of belief mass and is straightforward to parameterize using closed-form moments. The Generalized Dirichlet distribution extends this by introducing additional flexibility via a second set of parameters, enabling skewness and more complex belief shapes. Finally, the Beta stick-breaking model introduces an alternative constructive approach by allocating belief mass sequentially from Beta-distributed proportions, resulting in a valid but directionally expressive distribution over the simplex Stirn et al. (2019). All three models are fitted to the same belief mass vectors, and their sample distributions are visualized in Figures 7a, 7b, and 7c. While the Dirichlet and Generalized Dirichlet distributions align well with the center of mass observed in the belief functions, the Beta stick-breaking model demonstrates an equally valid fit but with a distinct shape and construction. This ablation supports the rationale that, while various PDFs on the simplex are valid for representing belief functions, the Dirichlet distribution remains a principled choice due to its mathematical simplicity, interpretability and established use in modelling epistemic uncertainty in neural networks.

Effect of Budgeting Set Size: Table 5 presents the classification accuracy of the Epistemic Wrapper on MNIST across varying budgeting percentages, both before and after fine-tuning. The percentage indicates the fraction of posterior weights selected for wrapping based on a high-mean criterion, while the number of intervals was fixed at 30. Before fine-tuning, we observe that moderate budgeting (e.g., 10% or 20%) results in significantly improved performance over the baseline INN, which achieved only 9.33% accuracy. In particular, wrapping only 10% of the weights led to a substantial increase in accuracy (45.34%), indicating that even a small subset of informative weights contributes meaningfully to uncertainty-aware decision-making. However, performance declines when budgeting exceeds 20%, which may be attributed to the limited capacity of the small-scale MLP model (with only 8 hidden units). In such a constrained architecture, wrapping a larger fraction of weights may reduce generalization by overfitting or introducing excessive variance in the wrapped ensemble.

1134
1135 Table 5: Performance comparison on MNIST across different budgeting percentages before and after
1136 fine-tuning.
1137

STRATEGY	INN ACCURACY (%)	EPI-WRAPPER BUDGETING PERCENTAGE (SELECTED WEIGHTS)					
		5%	10%	20%	30%	40%	50%
BEFORE FINE-TUNING	9.33 \pm 0.54	25.46 \pm 1.57	45.34 \pm 1.38	42.25 \pm 1.26	32.62 \pm 2.00	19.07 \pm 0.80	14.08 \pm 0.94
AFTER FINE-TUNING	91.12 \pm 0.08	91.08 \pm 0.09	91.83 \pm 0.04	91.84 \pm 0.04	91.85 \pm 0.13	91.82 \pm 0.09	91.50 \pm 0.05

1142
1143
1144 After fine-tuning, performance improves and stabilizes across all budgeting levels. The accuracy
1145 remains consistently above 91% even with minimal weight wrapping, indicating that fine-tuning
1146 effectively adjusts the selected wrapped weights to better align with the underlying predictive task.
1147 The best performance (91.85%) is achieved at 30% budgeting, but all configurations from 10% to
1148 50% perform comparably well, highlighting the robustness of the approach after refinement. These
1149 results confirm that wrapping a small subset of epistemically informative weights can significantly
1150 enhance predictive performance.
1151

1152 **Effect of Number of Closed Intervals:** To assess the impact of closed intervals for computing
1153 belief values leading to fitting a Dirichlet distribution over grid of mass values (as explained in
1154 sections 3.3 and 3.4). We conducted an ablation study by varying the number of intervals before
1155 fitting the Dirichlet distribution. Table 6 and Fig. 8 show the resulting α values computed using the
1156 method of *L-moments* for different numbers of intervals, with a fixed sample size of 5000. We observe
1157 that the estimated parameters stabilize around 30 intervals, beyond which changes become marginal.
1158 Based on this observation, we fix the number of intervals to 30 for all subsequent experiments to
1159 balance estimation stability and computational efficiency.
1160

1161 All ablation experiments are conducted on the MNIST dataset using a BNN MLP (hidden units= 8,
1162 samples =5000).
1163

1164 Table 6: Ablation study of Dirichlet α estimates using method of L-moment across varying numbers
1165 of intervals. Results are computed on 5000 samples.
1166

Number of Intervals	Estimated α Values
10	[1.0657, 4.5643, 1.0626]
20	[1.5958, 5.7176, 1.4097]
30	[1.6651, 6.1145, 1.6197]
40	[1.5272, 6.2213, 1.5665]
50	[1.6660, 6.3547, 1.6410]
60	[1.6935, 6.4927, 1.6669]

1174 C.2 FINE-TUNING USING WRAPPER WEIGHTS

1175
1176 Fine-tuning is an essential stage of the Epistemic Wrapper pipeline. Once the second-order represen-
1177 tation is constructed and the INN is initialised with Dirichlet-derived (wrapped) and Gaussian-derived
1178 (unwrapped) interval weights, the network must be adapted to the classification task under this new
1179 parameterisation. Fine-tuning restores discriminative performance while preserving the epistemic
1180 structure introduced by the Wrapper. The purpose of our method is therefore improved epistemic-
1181 aleatoric separation, calibration, interpretability, and OOD robustness-not state-of-the-art accuracy.
1182

1183 During inference, the INNs operate with two types of weights (as explained in section 3.5): ‘un-
1184 wrapped’ weights, directly sampled from Gaussian posteriors, and ‘wrapped’ weights that are
1185 Dirichlet-derived intervals. Specifically, for a given unwrapped weight with mean μ and standard
1186 deviation σ , we define the interval as:
1187

$$\text{Lower Bound} = \mu - k \cdot \sigma, \quad \text{Upper Bound} = \mu + k \cdot \sigma,$$

1188 where k is a learnable, layer-specific scaling factor.
1189

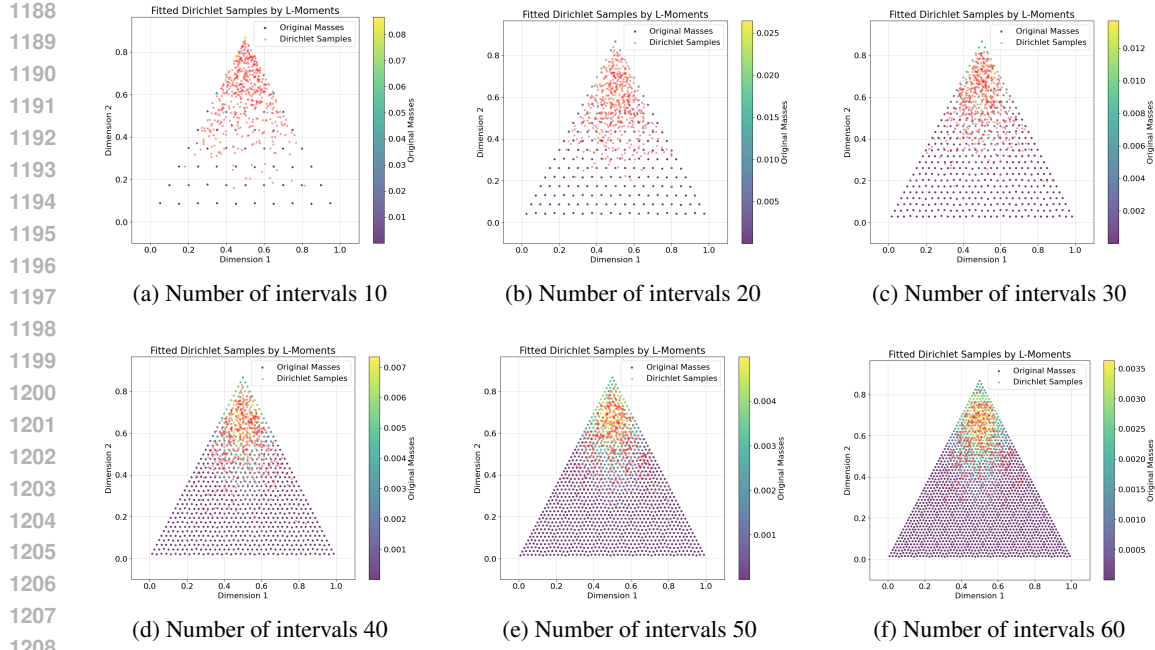


Figure 8: Varying Number of closed intervals

This scaling factor k serves a similar purpose to the *tempering parameter* τ in variational Bayesian inference Osawa et al. (2019), which modulates the influence of the likelihood in the posterior. Smaller values of k lead to narrower (sharper) intervals, corresponding to more confident parameter estimates; larger values encourage wider bounds and more conservative uncertainty. Unlike fixed-scale approaches (e.g., $\mu \pm \sigma$), our model learns k jointly with the rest of the parameters during training. For numerical stability and positivity, we parameterize k via a softplus transformation: $k = \log(1 + \exp(k_{\text{raw}}))$, where k_{raw} is a trainable tensor. This uncertainty calibration mechanism allows each layer to adaptively control the initial spread of its weights, improving both optimization stability and predictive robustness. This is especially important in deep architectures, where poorly controlled interval propagation may lead to unstable gradients or diluted information. At inference time, our method uses these calibrated intervals to propagate uncertainty. In contrast, the baseline INN applies standard random initialization Kim (1993). Both models undergo fine-tuning, but only the Epi-Wrapper benefits from interval-aware initialization based on transformed posteriors.

C.3 HYPERPARAMETER SETTINGS

The experimental setup of the main manuscript contains fixed hyperparameters such as number of closed intervals (30) and samples drawn from posterior distributions (5000). The budgeting strategy is applied consistently across experiments, with 5% of weights selected for small-scale model such as MLP, and 0.1% for larger architectures including LeNet-5, ResNet-18, and VGG-16.

C.4 ROC AND PRC COMPUTATION FOR OOD DETECTION

Scores and Labels. Given in-distribution (ID) samples with scores $\{s_i^{\text{id}}\}_{i=1}^{n_{\text{id}}}$ and out-of-distribution (OoD) samples with scores $\{s_j^{\text{oob}}\}_{j=1}^{n_{\text{oob}}}$, we form

$$\mathbf{s} = [s_1^{\text{id}}, \dots, s_{n_{\text{id}}}^{\text{id}}, s_1^{\text{oob}}, \dots, s_{n_{\text{oob}}}^{\text{oob}}], \quad \mathbf{y} = [0, \dots, 0, 1, \dots, 1],$$

where $y = 1$ denotes OoD and $y = 0$ denotes ID. In your code, each score is the predictive entropy

$$H(p) = - \sum_{c=1}^C p_c \log p_c,$$

computed from midpoint logits (averaging two heads) followed by softmax.

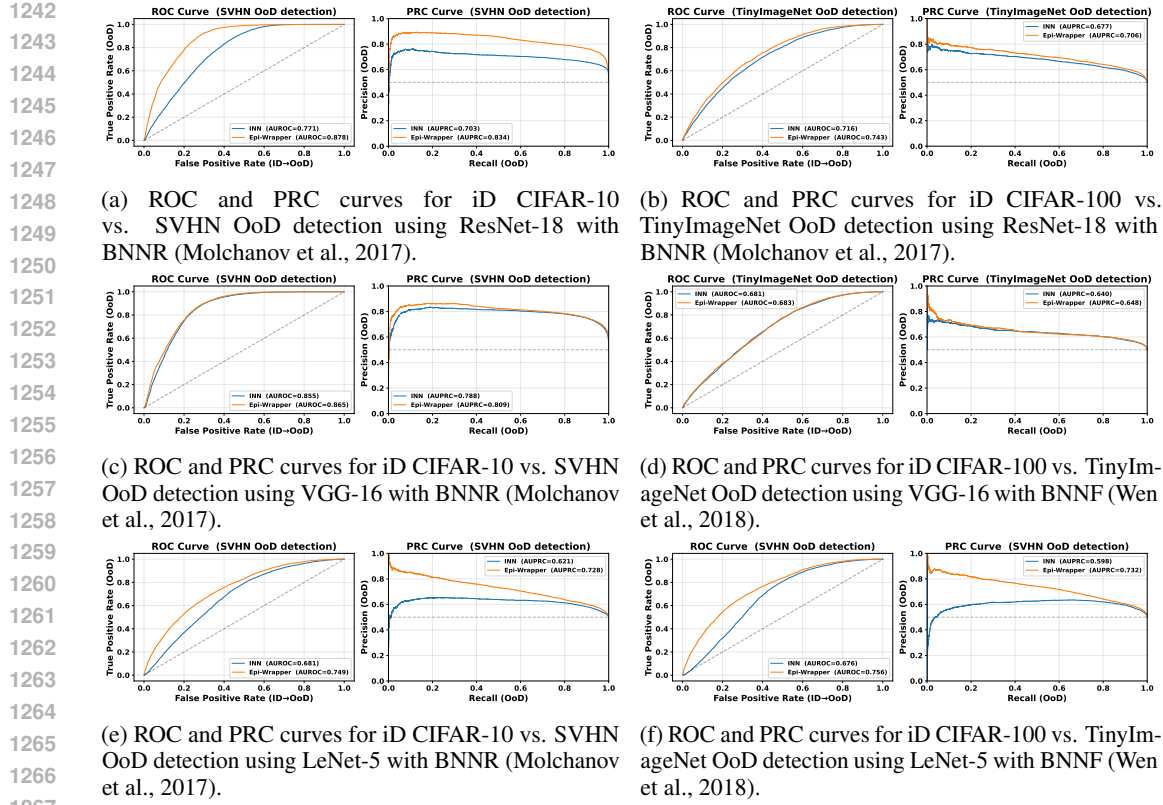


Figure 9: ROC and PRC results for OoD detection on SVHN dataset using INN and Epi-Wrapper. The curves illustrate performance trade-offs under entropy-based scoring, with AUROC and AUPRC values reported in the legends.

ROC: For a threshold τ , predict $\hat{y} = \mathbb{I}[s \geq \tau]$. Define

$$TPR(\tau) = \frac{TP(\tau)}{TP(\tau) + FN(\tau)}, \quad FPR(\tau) = \frac{FP(\tau)}{FP(\tau) + TN(\tau)}.$$

Sweeping τ from $+\infty$ to $-\infty$ traces the ROC curve $(FPR(\tau), TPR(\tau))$. The area under the ROC (AUROC) is computed by the trapezoidal rule over the curve.

PRC: Precision–Recall uses

$$\text{Precision}(\tau) = \frac{TP(\tau)}{TP(\tau) + FP(\tau)}, \quad \text{Recall}(\tau) = TPR(\tau).$$

Sweeping τ yields the PRC $(\text{Recall}(\tau), \text{Precision}(\tau))$. The area under the PRC (AUPRC) can be computed via the average-precision estimator or trapezoidal integration. A reference baseline is the positive prior $\pi = \frac{n_{\text{oob}}}{n_{\text{id}} + n_{\text{oob}}}$.

Comparative Analysis. The ROC and PRC plots in Figure 9 further highlight the performance differences between INN and Epi-Wrapper on OoD detection with SVHN as the outlier dataset. Across both backbone settings (ResNet-18 with BNNF and VGG-16 with BNNR), the Epi-Wrapper curves consistently dominate the INN baseline, reflecting higher true positive rates at lower false positive rates in ROC space, as well as improved precision across recall levels in PRC space. These visual trends align with the quantitative results reported in Table 3, confirming that parameter-space uncertainty modeling via Epi-Wrapper yields superior separability between in-distribution and out-of-distribution samples. The improvement is particularly pronounced in the PRC, where Epi-Wrapper maintains high precision even at challenging recall levels, suggesting its robustness under class-imbalance conditions common in OoD detection tasks.

1296 Table 7: ECE and NLL for INN (baseline) vs. Epi-Wrapper (ours) across MNIST, Fashion-MNIST,
 1297 CIFAR-10, and CIFAR-100 datasets using BNNF and BNNR baselines with MLP, LeNet-5, ResNet-
 1298 18, and VGG-16 backbones. (Classification accuracy results are reported separately in Table 2.)
 1299
 1300

1301 DATASET	1302 BACKBONE	# PARAMS	1303 BASELINE	ECE (↓)		NLL (↓)	
				1304 INN	EPI-WRAPPER	1305 INN	EPI-WRAPPER
MNIST	MLP	12.7K	BNNF	0.011 ± 0.031	0.009 ± 0.018	0.388 ± 0.007	0.298 ± 0.004
FASHION MNIST	MLP	12.7K	BNNF	0.035 ± 0.012	0.006 ± 0.090	0.410 ± 0.018	0.332 ± 0.019
CIFAR-10	LENET-5	166.3K	BNNF	0.060 ± 0.061	0.059 ± 0.019	1.365 ± 0.090	1.210 ± 0.045
			BNNR	0.060 ± 0.061	0.053 ± 0.006	1.365 ± 0.090	1.608 ± 0.009
	RESNET-18	9.82M	BNNF	0.084 ± 0.015	0.041 ± 0.013	0.616 ± 0.070	0.333 ± 0.012
CIFAR-100	VGG-16	30.24M	BNNF	0.073 ± 0.012	0.069 ± 0.087	0.520 ± 0.081	0.451 ± 0.033
			BNNR	0.073 ± 0.012	0.071 ± 0.010	0.520 ± 0.081	0.462 ± 0.054
	RESNET-18	9.8M	BNNF	0.059 ± 0.049	0.055 ± 0.087	1.460 ± 0.084	1.451 ± 0.088
CIFAR-100	VGG-16	30.24M	BNNR	0.059 ± 0.049	0.051 ± 0.056	1.460 ± 0.084	1.437 ± 0.010
			BNNF	0.043 ± 0.023	0.040 ± 0.013	2.141 ± 0.089	1.999 ± 0.071
			BNNR	0.043 ± 0.023	0.039 ± 0.045	2.141 ± 0.089	1.766 ± 0.059

1314 C.5 CALIBRATION AND LIKELIHOOD EVALUATION

1316 To evaluate the probabilistic calibration of our models, we compute two key metrics: ‘Expected
 1317 Calibration Error (ECE)’ and ‘Negative Log Likelihood (NLL)’. These metrics assess the alignment
 1318 between predicted confidence and actual correctness (ECE), and the quality of probabilistic
 1319 predictions (NLL).

1320 **Expected Calibration Error (ECE):** quantifies the average discrepancy between the predicted
 1321 confidence of a model and the observed precision. Predictions are binned into M intervals (we use
 1322 $M = 15$). For each bin, the average confidence and accuracy are computed, where $\text{conf}(B_m)$ is the
 1323 average predicted maximum probability of samples in bin B_m . The ECE is the weighted average of
 1324 the absolute difference between these values across all bins:

$$1325 \quad 1326 \quad 1327 \quad 1328 \quad \text{ECE} = \sum_{m=1}^M \frac{|B_m|}{n} |\text{acc}(B_m) - \text{conf}(B_m)|, \quad (13)$$

1329 where n is the total number of samples, and B_m denotes the m -th bin.

1330 **Negative Log Likelihood (NLL):** captures how well a model’s predicted probabilities match the true
 1331 labels. It penalizes incorrect predictions with high confidence and rewards well-calibrated probability
 1332 distributions:

$$1333 \quad 1334 \quad 1335 \quad \text{NLL} = -\frac{1}{n} \sum_{i=1}^n \log \hat{p}_{i,y_i}, \quad (14)$$

1336 where \hat{p}_{i,y_i} is the predicted probability for the correct class.

1337 Table 7 summarizes the performance of the baseline INN and the proposed Epi-Wrapper model on
 1338 the four datasets. Across almost all settings, Epi-Wrapper achieves lower ECE and NLL compared to
 1339 the INN baseline, highlighting its superior probabilistic calibration and confidence estimation. These
 1340 improvements suggest that, beyond classification accuracy, Epi-Wrapper provides more trustworthy
 1341 uncertainty estimates, which is especially important for decision-critical applications where model
 1342 confidence is as crucial as prediction correctness.

1343 D MODELING EPISTEMIC UNCERTAINTY: PARAMETER VS. TARGET SPACE

1344 Epistemic uncertainty (EU) originates from limited knowledge about the model parameters them-
 1345 selves, a view grounded in Bayesian learning where posterior distributions over weights directly
 1346 encode parameter uncertainty. Although several recent approaches such as Evidential Deep Learning
 1347 (EDL) (Sensoy et al., 2018) and credal set-based classification (Wang et al., 2024b) have focused
 1348 on modeling uncertainty in the target (output) space, these methods do not explicitly represent

1350 uncertainty over model parameters. In contrast, our Epistemic Wrapper framework introduces a
 1351 second-order uncertainty representation in the parameter space via belief functions. By wrapping
 1352 posterior distributions derived from BNNs, our approach captures variability before the prediction
 1353 stage, allowing for richer epistemic modeling. This can be particularly beneficial in scenarios with
 1354 limited training data or when encountering out-of-distribution (OoD) inputs.

1355 Approaches that operate solely in the output space such as decompositions of predictive uncertainty
 1356 via proper scoring rules, Bregman divergences, calibration methods, or generalized bias-variance
 1357 analyses (Kotelevskii et al., 2024; Ahdritz et al., 2024; Gruber & Buettner, 2022) provide important
 1358 insights into the behaviour of predictive distributions. However, these techniques characterize EU only
 1359 indirectly, after uncertainty has already propagated through the model. In contrast, our framework
 1360 addresses uncertainty at its source by representing and enriching parameter-space posteriors before
 1361 they influence predictions. This distinction allows us to capture model-level uncertainty in a principled
 1362 way, offering a complementary perspective to output-based decompositions. By integrating belief
 1363 functions and Dirichlet representations directly in parameter space, our method provides a prior-
 1364 agnostic and interpretable mechanism for epistemic uncertainty quantification, while remaining fully
 1365 compatible with existing Bayesian neural networks.

1366 We stress that parameter-space and target-space approaches are not substitutes but complementary
 1367 perspectives. Target-space methods characterize predictive uncertainty directly, while parameter-
 1368 space methods quantify the model’s internal epistemic state before it influences predictions. Our
 1369 experiments show that Epistemic Wrapper consistently improves on standard downstream tasks
 1370 such as OoD detection, calibration (ECE), and likelihood evaluation (NLL), providing strong em-
 1371 pirical evidence that parameter-space epistemic modeling yields practical benefits in addition to
 1372 its theoretical grounding. In summary, Epistemic Wrapper serves as a principled complement to
 1373 target-based methods, enriching parameter-space uncertainty modeling. Importantly, our method is
 1374 not directly comparable to target-based approaches such as EDL or ensembles, because they operate
 1375 in a fundamentally different space.

E EPI-WRAPPER FOR REGRESSION TASKS

1379 In principle, the Epistemic Wrapper is not restricted to classification tasks. The proposed framework
 1380 models epistemic uncertainty in the parameter space of Bayesian Neural Networks via belief functions,
 1381 which is independent of the nature of the output space. The only requirement for extending the
 1382 method to regression tasks is the availability of a suitable Interval Neural Network (INN) or similar
 1383 regression architecture capable of consuming interval-valued parameters during inference. While we
 1384 have focused on classification tasks in this work, we believe that extending the approach to regression
 1385 is a natural and promising direction for future work.

1386
 1387
 1388
 1389
 1390
 1391
 1392
 1393
 1394
 1395
 1396
 1397
 1398
 1399
 1400
 1401
 1402
 1403